Desalination and Water Treatment
www.deswater.com
doi: 10.5004/dwt.2022.28643

267 (2022) 26–44
August

Magnetic nanocomposite of zinc–manganese ferrite/polyurethane foam for adsorption of copper and cadmium from water

Sami M. Abdel Azeem[a,b,*], Mohamed M.S. Wahsh[c], Fatma H. Youssef[a], Ahmed M.H. Ibrahim[b,d], Nagwa Burham[a]

[a]*Chemistry Department, Faculty of Science, Fayoum University, Egypt, Tel. +20 1207664342; Fax: +20 846370025; email: sma13@fayoum.edu.eg (S.M. Abdel Azeem), Tel. +20 1066019065; email: hfatma106@gmail.com (F.H. Youssef), Tel. +20 1283877751; email: n_burham@yahoo.com (N. Burham)*

[b]*Chemistry Department, Al-Quwayiyah College of Science and Humanities, 11971, Shaqra University, Saudi Arabia, email: sami_a@su.edu.sa (S.M. Abdel Azeem)*

[c]*Refractories, Ceramics and Building Materials Department, National Research Centre, 12622, El-buhouth St., Dokki, Cairo, Egypt, Tel. +201007561987; Fax: +20 233370931; email: mmswahsh@yahoo.com (M.M.S. Wahsh)*

[d]*Hot Laboratory Centre, Fuel Technology Department, Atomic Energy Authority, Abu-Zabal-Kalubia P.O. 13759, Egypt, email: a.ibrahim@su.edu.sa (A.M.H. Ibrahim)*

Received 22 February 2022; Accepted 29 June 2022

ABSTRACT

The magnetic nanoparticles, zinc–manganese ferrite ($Zn_{0.6}Mn_{0.4}Fe_2O_4$), were chemically added to polyurethane foam (PUF) to obtain the polymeric nanocomposite $Zn_{0.6}Mn_{0.4}Fe_2O_4$/PUF. Characterization of the nanoparticles and the nanocomposite was made by X-ray diffraction, scanning electron microscopy, high-resolution transmission electron microscopy, and vibrating sample magnetometer. The prepared nanocomposite showed adsorption efficiency of 95% and 94% for Cu and Cd, respectively at a pH of 6.5, a shaking time of 60 min, and a composite dosage of 0.2 g. Adsorption kinetics followed a second-order model, with k_2 = 3.02 and 4.05 mg g^{-1} min^{-1} and adsorption capacity was 20.4 and 11.1 mg g^{-1}, respectively. The Freundlich model best described the adsorption isotherm, n = 0.93 and 0.88 and K_F = 0.64 and 0.31 L g^{-1}, and R^2 = 0.988 and 0.980, respectively. The quantification limits are 0.9 and 1.4 µg L^{-1}, respectively, with a preconcentration factor of 125. The removal of Cd and Cu from tap, lake and river waters, yielding a recovery from 89%–116% relative standard deviation (RSD = 0.8%–8.6%).

Keywords: Zinc–manganese ferrite nanoparticles; Polyurethane foam; Nanocomposite sorbent; Copper and cadmium; Lake, river and tap waters

1. Introduction

Heavy metal pollution of water has become a major concern because of the dangers that these contaminants pose to human health and the environment [1]. Copper (Cu) is toxic to human health due to its adverse effects on the kidney, liver, and gastrointestinal tract [2]. It imparts an unpleasant taste to drinking water at a 3 mg L^{-1} concentration and can cause illness in susceptible people at a 2 mg L^{-1} level [3]. Cadmium (Cd) intake from water in a long-term can damage the kidney, liver, bone, and, blood [4]. The World Health Organization (WHO) has set the maximum contamination limit (MCL) for Cu and Cd in drinking water at 2.0 and 0.003 mg L^{-1}, respectively [5]. Effective and cost-effective methods for removing Cu(II) and Cd(II) from water are thus critical issues.

---

* Corresponding author.

Several adsorbents have been used for the adsorption/removal of Cu and Cd from aqueous solutions, including bentonite [6], potassium titanate whiskers [7], chitosan beads-manganese ferrite ($MnFe_3O_4$) [8], magnetic iron-modified calcium silicate hydrate [9], coal fly ash zeolite [10] and polyvinyl alcohol/bacterial cellulose/calcium carbonate composite [11]. Adsorption was deemed superior among these technologies because of its ease of operation, high removal efficiency, cost-effectiveness, and availability of effective sorbents [12,13].

Nanomaterials have received considerable recognition because of their uniform and consistent complexity with functional groups, tunable pores, and high selectivity and sensitivity [14]. Nano-carbon, nano-metal oxide, maghemite, dendrimers, and alginate nanoparticles are conventional nanosorbents for Cu(II) and Cd(II) removal [15,16]. Magnetic nanosorbents are gaining popularity in the removal of heavy metals and dyes due to their large surface area, limited diffusion resistance, and fast magnetic separation [17,18]. However, these nanosorbents usually have the drawback of taking a long time to adsorb the analyte from the adsorbent and having a high separation cost, which severely restricts the usage [19,20].

Spinel ferrites, $MeFe_2O_4$ (Me = Mg, Ni, Cu, Mn, Co, Zn)-based nanosorbents have been commonly used for the removal of heavy metals from the aqueous phase due to their unique properties such as chemical stability and substantial magnetic permeability [21–23].

Zinc ferrite ($ZnFe_2O_4$) belongs to the cubic spinel ferrite family, and it has good crystallinity and magnetic properties, which are important factors in reviving a sorbent from a treated solution using an external magnetic field [24–27]. Manganese ferrite ($MnFe_2O_4$) is a well-known sorbent with a high propensity for ion binding [28,29]. Furthermore, during various toxicity studies, $MnFe_2O_4$ in the nanostructure form shows no toxicity effect, suggesting that it can be used as a good alternative to other iron-based adsorbents in the removal of toxic metal ions from the aqueous phase [30,31].

Manganese zinc ferrite has the formula $(A)[B]_2O_4$ that describes a cubic spinel configuration, where (A) and [B] refer to tetrahedral and octahedral cation sites, respectively. Many of the intrinsic magnetic properties of the ferrite are determined by the type of cations and their distribution between the two interstitial ferrite sites. Interestingly, certain nanocrystalline spinel ferrites have distinct cation distributions; as a result, their magnetic properties differ from their bulk counterparts. The equilibrium distribution of cations in the spinel structure is affected by the ionic radius, electron configuration, electrostatic energies, and polarization effects [32]. Regrettably, the ferrite's surface area was found to be limited, which may be a limiting factor in the adsorption process. The modification of the non-magnetic portion of the ferrite increases its potency by increasing the surface area usable for adsorption. By adding manganese to ferrite, it increases the adsorption performance of heavy metals by providing more stability and improving the surface area [32]. The ferrites' adsorption properties are determined by their structure and composition, which in turn depend on the production technique and cation dispersion in the crystal lattice [33]. As a result, the choice of combined zinc and manganese ferrites as an adsorbent for Cd and Cu is based on the ability to tolerate the ferrite's magnetic characteristics to obtain saturated electromagnetization with high potency for metal ion binding as well as good sorbent permeability and stability. Furthermore, the existence of tetrahedral and octahedral interstitial spaces in the spinel structure allows the investigated metal ions to enter the crystal lattice by replacing Fe(III) ions, resulting in metal ion aggregation on the grain boundary [34].

Organic polymers contain a large number of multifunctional groups that can efficiently adsorb heavy metal ions, but their low adsorption rate limits their use. A high surface area and abundant functional groups are crucial properties of an efficient adsorbent, in addition to high capacity and quick adsorption [35].

Polyurethane foam (PUF) is a versatile polymer with a highly usable surface area and an incredibly low cost. It is acid and base stable and will not change composition when heated to 180°C. As a result, it is an excellent material for preconcentration and separation techniques [36]. PUF has been used as a sorbent for Cu and Cd preconcentration and separation, either untreated [37], grafted with cationic dyes [38], or functionalized with chelating reagents via azo (–N=N–) [39] or imine (–C=N–) [40]. Polymeric nanocomposites combine the special properties of polymers such as flexibility, ductility, and processability with the benefits of inorganic nanofillers such as rigidity and thermal resilience [41]. For the adsorption/removal of Cu and/or Cd, several polymeric nanocomposites sorbents were used, including graphene oxide modified with magnetite nanoparticles and Lauric acid-containing ethylenediaminetetraacetic acid [42] and PUF-organobentonite/iron oxide [43].

In this work, we aimed to develop a novel highly porous $Zn_{0.6}Mn_{0.4}Fe_2O_4$/PUF nanocomposite adsorbent for the adsorption of Cu and Cd from water by chemically embedding magnetic nanoparticles of $Zn_{0.6}Mn_{0.4}Fe_2O_4$ into the backbone of PUF polymer. PUF was chosen as a support because of its high surface area, expected ability to reduce nanoparticle agglomeration via foaming reaction, and ease of separation of the adsorbent from the water after adsorption. The following were the objectives of this work: (1) to prepare and characterize the nanocomposite adsorbent using various analytical tools like Fourier-transform infrared spectroscopy (FT-IR), X-ray diffraction (XRD), scanning electron microscopy (SEM), high-resolution transmission electron microscopy (HR-TEM), and Brunauer–Emmett–Teller (BET). (2) to determine the nanocomposite's adsorption performance and removal efficiency for Cu and Cd ions from aqueous solutions by examining parameters such as solution pH, adsorbent dosage, and adsorption kinetics and isotherms. (3) To apply the adsorbent to remove the studied elements from real water samples like a tap water, Qaroun Lake, and Yousef River.

2. Experimental

2.1. Instrumentation

The FT-IR spectra of the untreated PUF, $Zn_{0.6}Mn_{0.4}Fe_2O_4$/PUF nanocomposite were recorded using a PerkinElmer 1750 Fourier Transform Infrared Spectrometer (Boston, MA, USA). The spectrum of a Cu(II)-loaded nanocomposite from a 2.0 mg L^{-1} solution at pH 6.5 and 0.2 g of adsorbent was also examined. The powdered samples were made using the KBr discs approach and recorded in the wavenumber range of 400–4,000 cm^{-1}. Micromeritics' Gemini VII Surface Area Analyzer Model 2390T V1.03 was used to perform BET surface area and pore analysis (GA, USA). N_2 adsorption was assessed on a surface characterization device with a dray sample weighing 0.02 g and a density of 1.00 g cm^{-3} at 77 K and a relative pressure (P/Po) in the range of 0.05–0.8. The samples were degassed for 2 h at 120°C before the measurements.

An XRD pattern was recorded on the Bruker D8 ADVANCE Diffractometer (Berlin, Germany) with Cu-Kα1 anode λ = 1.54058 Å radiation and a secondary monochromator at a scanning speed of 1°/min^{-1} for studying the phase composition and average crystallite size of the magnetic nanoparticles. A Lakeshore VSM 7410 vibrating sample magnetometer (Texas, USA) equipped with 3T magnets was used to measure the magnetic properties of the prepared ferrite nanoparticles. HR-TEM images were taken using a JEOL transmission electron microscope model JEM-2100 (Tokyo, Japan) to observe the morphology and particle size of the nanocomposite material. The FEI scanning electron microscope (SEM) model Quanta™ FEG-250 (Oregon, USA) was used to show the microstructure of the prepared nanocomposite material. Agilent flame atomic absorption spectrometer (FAAS) model FAA-55 (CA, USA) equipped with single element hollow cathode lamps and an air-acetylene burner was used for the determination of Cd and Cu elements. The BOECO Microprocessor pH Meter model BT 500 (Hamburg, Germany) calibrated against standard buffer solutions at pH 4 and 9 was employed for the pH adjustments. A SL 350 Nuve Mechanical Shaker (Akyurt, Ankara, Turkey) with up to 200 rpm and speed control was used to shake the samples. Double distilled water (DDW) was obtained from a Hamilton Laboratory Glass Instrument (Europe House, Sandwich Industrial Estate, Sandwich, Kent, England).

2.2. Chemicals and reagents

All reagents used were of analytical reagent grade, and the standard solutions were prepared in DDW. Cadmium nitrate tetrahydrate $Cd(NO_3)_2{\cdot}4H_2O$ from Panreac Co., (Barcelona, Spain) and cupric sulfate pentahydrate $CuSO_4{\cdot}5H_2O$ from Aldrich (Milwaukee, USA) were used to prepare the standard metal ion solutions. Sodium hydroxide (NaOH) and hydrochloric acid (HCl) were obtained from El-Nasr Pharmaceutical Chemicals Co., Adwic (Cairo, Egypt) and used for pH adjustment.

Ferric nitrate nonahydrate $Fe(NO_3)_3{\cdot}9H_2O$ from Alpha Chemika™ (Mumbai, India), zinc nitrate hexahydrate $Zn(NO_3)_2{\cdot}6H_2O$ from WinLab (Brendale, Australia), manganese nitrate tetrahydrate $Mn(NO_3)_2{\cdot}4H_2O$ from Sigma-Aldrich (Missouri, USA), citric acid monohydrate gritty $C_6H_8O_7{\cdot}H_2O$ from Riedel-de Haën (Sleez, Germany) and a 30% (v/v) ammonia solution (NH_4OH) from Sigma-Aldrich, were used to prepare the magnetic nanoparticles.

Polyol (Polyether type), stannous octoate, silicone oil, and toluene diisocyanate (TDI) were kindly received from the Egyptian Foam Co. (Cairo, Egypt) and utilized to prepare the PUF.

The stock solutions of Cd(II) and Cu(II) were prepared at a concentration of 1,000 mg L^{-1} by weighing appropriate amounts of cadmium nitrate and cupric sulfate. Each reagent was dissolved in 1,000 mL of double distilled water, with 2.0 mL of concentrated nitric acid added to prevent metal ion hydrolysis. Working solutions were prepared by diluting the stock solution to the desired concentrations in the range of 0.1–10 mg L^{-1}. The pH of the samples was adjusted with HCl and NaOH solutions at suitable concentrations.

2.3. Synthesis of the polymeric nanocomposite sorbent

2.3.1. Preparation of the magnetic nanoparticles

The magnetic nanopowder ($Zn_{0.6}Mn_{0.4}Fe_2O_4$) was synthesized using a modified citrate sol–gel combustion method [44]. Zinc nitrate, manganese nitrate, and ferric nitrate solutions each at a concentration of 0.25 mol L^{-1} were prepared by dissolving 0.372, 0.314, and 0.505 g of the metal nitrate in 50 mL of DDW. The Mn^{2+} and Zn^{2+} solutions were mixed together in 40 and 60 mL volumes, corresponding to a molar ratio of 0.4 and 0.6, respectively. After that, the Fe^{3+} solution (50 mL) was added under steady stirring to an equivalent volume of the previous mixture, yielding a molar ratio of Me^{2+}/Fe^{3+} = 0.5, where Me^{2+} represents the total concentration of Mn^{2+} and Zn^{2+}. The homogeneous solution that resulted was heated at a rate of 5°C/min^{-1} up to 80°C for 1 h. Next, the heated mixture was added to a 100 mL of 0.25 mol L^{-1} citric acid solutions, maintaining the concentration of the total metal ions and citric acid at a molar ratio of 1:1 and stirring for 2 h. Thereafter, the ammonia solution was added to the agitating mixture to raise the pH value to approximately 7.5. During the stirring process, an increasing temperature contributes to the formation of a viscous gel. The ignition process started at the proper temperature and the formed gel burned itself, propagating the manner of combustion until all the gel was fully burnt out to form a fine powder. Finally, the prepared powder was fired for 1 h at 400°C to give the $Zn_{0.6}Mn_{0.4}Fe_2O_4$ nanopowder.

2.3.2. Embedding of the magnetic nanoparticles in PUF

The nanocomposite, which is composed of nanoparticles embedded in PUF, was created by incorporating the nanoparticles into the previously described PUF synthesis technique [38]. To begin, a selected amount of 0.1 g of $Zn_{0.6}Mn_{0.4}Fe_2O_4$ nanopowder was mixed with 20 g of polyol (polyether) and thoroughly mixed until it was completely homogenous, after which 0.04 g of stannous octoate was applied and stirring was resumed. Following that, a 13.5 g toluene diisocyanate (TDI) was progressively applied while vigorously stirring, followed by 3 drops of silicon oil, at which point the foaming liquid polymer began to form, and 2 mL of purified water was added, causing the foaming mixture to expand. The nanocomposite foaming mixture is then poured into a box with a fitted lid, allowing for the homogenous dispersion of the emerging carbon dioxide blowing gas. After allowing the foam to solidify at room temperature, it was cut into small cubes and treated with 1.0 mol L^{-1} HCl to remove inorganic impurities before being washed with double distilled water and dried at room temperature.

2.4. Batch adsorption procedure

In the batch process, a certain amount of 0.2 g nanocomposite sorbent is added to a 25 mL sample containing a metal ion concentration of 0.8 mg L^{-1} adjusted to pH 6.5, and the mixture is shaken for 60 min with a mechanical shaker. Filtration is used to isolate the sorbent along with the extracted elements from the liquid sample. The adsorbed metal ions are then recovered from the sorbent by shaking with a 10 mL eluate of 0.5 mol L^{-1} HCl solution. Finally, the concentration of the recovered metal ions was quantified using the recommended FAAS technique. The adsorption percentage of metal ion was calculated by using the following equation:

$$\text{Adsorption}\left(\%\right)=\left[\frac{\left(C_o-C\right)}{C_o}\right]\times 100 \tag{1}$$

where C_o and C are the initial and remaining concentrations (μg L^{-1}) of the metal ion, respectively.

The effect of pH on Cd(II) and Cu(II) sorption was studied within a pH range of 2.0–8.0 using NaOH and HCl solutions. The sorbent dose was investigated from 0.05 to 0.3 g. The effect of shaking time was varied from 1 to 60 min at the optimized pH and sorbent amount. Eq. (2) was used to calculate the amount of metal ion adsorbed (q, μg g^{-1}) at any time t.

$$q_t=\frac{\left[\left(C_0-C\right)\times V\right]}{m} \tag{2}$$

where V is the sample volume (L) and m is the weight of the nanocomposite sorbent (g).

Sorption isotherms were studied using various metal ion concentrations ranging from 0.2 to 3.6 mg L^{-1} concentrations of Cu(II) or Cd(II) in a 25 mL sample volume and 0.20 g sorbent weight. The maximum adsorption capacity ($q_{\max}$) of the nanocomposite sorbent was evaluated as the largest amount adsorbed when approaching equilibrium conditions and calculated according to Eq. (2).

A preconcentration study was performed using batch adsorption under optimized conditions of pH, sorbent weight, shaking time, and elution at different sample volumes ranging from 25–1,500 mL, containing a fixed amount of 20 μg of each metal ion. The recovery (%) was calculated by dividing the metal ion concentration (μg L^{-1}) found in the eluate by that found in the sample, as given by Eq. (3).

$$\text{Recovery}\left(\%\right)=\left[\frac{C}{C_o}\right]\times 100 \tag{3}$$

2.5. Determination of Cd and Cu by FAAS

In the FAAS determination of Cd and Cu elements, a single-element hollow cathode lamp and an air-acetylene burner were used. The flow rate of air-acetylene to the flame was 2 and 10 L min^{-1} for the fuel and oxidant, respectively, with a burner height of 10 cm. For Cd(II) determination, the slit width was set at 0.7 nm, replicates were set at 3.0, and read time was set at 3.0 s. The wavelengths and lamp current were selected at 228.8 nm and 10.0 mA, respectively. The regression equation was: $A = 0.0398C + 0.242$ ($R^2 = 0.995$). The slit width for Cu(II) was 0.7 nm, the replicates were 3, and the read time was 3.0 s. The wavelength and lamp current were set to 423.8 nm and 15.0 mA, respectively. The regression equation for Cu(II) determinations was $A = 0.0911C + 0.0030$ ($R^2 = 0.998$). Where A and C are the absorbance and concentration (mg L^{-1}), respectively.

2.6. Water samples

Three samples were collected from Fayoum City, Egypt: river, lake, and tap waters. The river water was collected from the Yousef River, which flows through the middle of Faiyum Governorate. It is a small branch that extends from the River Nile and serves as the main source of irrigation and feeds water to the main drinking plants. A lake water sample was collected from Qaroun Lake, one of the biggest natural lakes in Egypt, which is located about 27 km north of the Faiyum Governorate. Tap water was collected from our research laboratory at the Faculty of Science. A 3.0 L volume of each sample was taken and filtered to remove any suspended solids. The physico-chemical parameters of the water samples studied are listed in Table 1. Cu and Cd concentrations in the samples ranged from 35–47 and 5.0–7.7 μg L^{-1}, respectively. The collected samples were then acidified to pH 2.0 with nitric acid to avoid metal ion precipitation before being stored in sterile polyethylene bottles. A 100 mL water sample was spiked with an 800 μg L^{-1} level of the tested metal ions, and the mixture was mechanically shaken for 1 h. The adsorbed metal ions were eluted by shaking the loaded sorbent with 10 mL of 0.5 mol L^{-1} HCl solution. The concentration of each metal ion in the eluate was determined using the recommended FAAS method.

3. Results and discussion

3.1. Characterization of the nanocomposite sorbent

3.1.1. FT-IR analysis

The FT-IR spectra obtained are shown in the supplementary Fig. 1. The spectrum of untreated PUF (A) is complicated, having multiple absorption bands that could overlap with those of the implanted nanoparticles. Fig. 1B and C show broad absorption bands ranging from 538 to 512 cm^{-1}, corresponding to the stretching vibration of octahedral metal oxide (M–O) bonds for Fe–O, Mn–O, and Zn–O [45]. While for the untreated PUF, a narrow absorption band appeared at 511 cm^{-1}. The minor shift in the band from 1621 in PUF to 1590 in the nanocomposite is also noteworthy, showing that the amide part of the urethane group

Table 1
Physico-chemical parameters of the studied water samples

Property	Yousef River	Qaroun Lake	Tap water
pH	7.7	8.2	7.5
Conductivity, mS cm^{-1}	0.64	4.64	0.41
TDS, mg L^{-1}	390	2,790	243
Turbidity, NTU[a]	43	61	1.0
Chloride, mg L^{-1}	110	165	2.0
Sulfate, mg L^{-1}	57.0	11,874	28.0
Nitrate, mg L^{-1}	9.1	14.5	3.3
Ca, mg L^{-1}	124.0	438	85.0
Mg, mg L^{-1}	93.2	1,137	61.0
Cu, µg L^{-1}	45	47	35
Cd, µg L^{-1}	6.3	7.7	5.0

[a]Nephelometric turbidity unit

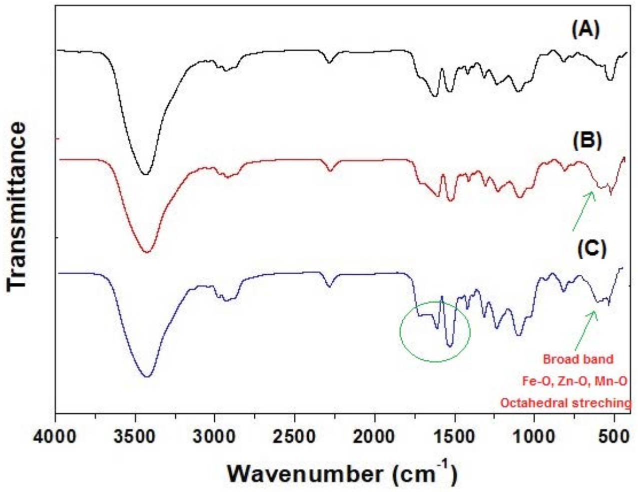

Fig. 1. FT-IR spectra of untreated PUF (A), $Zn_{0.6}Mn_{0.4}Fe_2O_4$/PUF nanocomposite (B) and Cu-loaded $Zn_{0.6}Mn_{0.4}Fe_2O_4$/PUF nanocomposite (C).

(–NH–CO–O–) is involved in nanoparticle embedding [8]. Furthermore, in the nanocomposite spectrum and following adsorption to Cu, a large increase in the absorption band at 1,510 cm^{-1} (attributed to the urethane C=O stretching in PUF) demonstrates the connecting of the ferrite metal ions and the tested elements to PUF via the urethane C=O bonding. This validated the nanoparticles' chemical incorporation into the polymer.

3.1.2. XRD analysis

Fig. 2 displays the XRD patterns of $Zn_{0.6}Mn_{0.4}Fe_2O_4$ nanoparticles (*A*) that were fired at 400°C for 1 h and for the $Zn_{0.6}Mn_{0.4}Fe_2O_4$/PUF nanocomposite material (*B*). The nanoparticles pattern showed main diffraction peaks at 2θ = 29.919°, 35.264°, 42.844°, 53.11°, 56.629°, 62.212°, and 73.513°, respectively, and were due to the crystal plane of the cubic spinel ferrites structure (220), (311), (400), (422), (511), (440) and (533) planes. The $Zn_{0.6}Mn_{0.4}Fe_2O_4$ nanoparticles were found to have the same crystal planes as $ZnFe_2O_4$ according to the XRD JCPDS (Joint Committee on Powder Diffraction Standards) data file No.22-1012 and $MnFe_2O_4$ (XRD JCPDS data file No.74-2403, indicating the formation of a good crystalline and single cubic phase of spinel structure. The average crystallite size of $Zn_{0.6}Mn_{0.4}Fe_2O_4$ nanoparticles was calculated using Debye–Scherrer's Eq. (4).

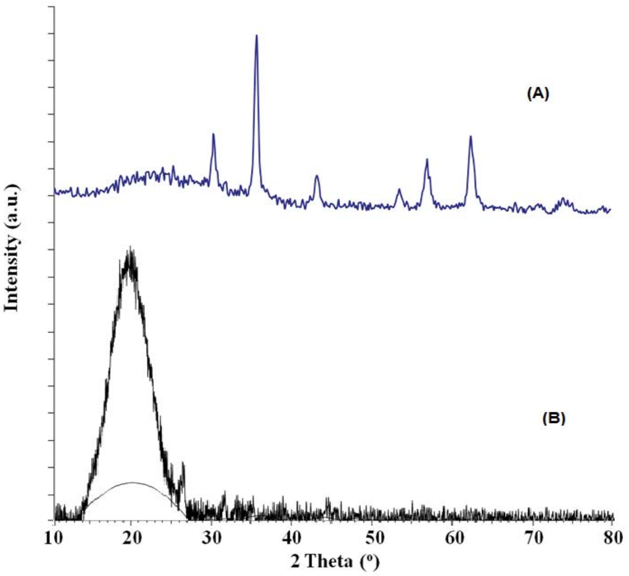

Fig. 2. XRD analysis of the prepared $Zn_{0.6}Mn_{0.4}Fe_2O_4$ nanoparticles (A) and after background correction for $Zn_{0.6}Mn_{0.4}Fe_2O_4$/PUF nanocomposite (B).

$$D = \frac{0.9\lambda}{\left(\text{FWHM} \times \cos\theta\right)} \quad (4)$$

where *D* is the crystallite size, FWHM is the observed full width at half maximum, θ is the Bragg angle, and λ is the X-ray wavelength (λ = 1.54058 Å). The XRD patterns indicated that the $Zn_{0.6}Mn_{0.4}O_4$ nanoparticles have an average crystallite size of 16.6 nm.

In the nanocomposite pattern (*B*), there are strong peak reductions and also some peaks that appear to be quite low, which could be owing to the low amount of the embedded nanoparticles. Also, a deviation was observed in the diffraction peaks with a value of $2\theta = 1.5°–2.0°$.

3.1.3. HR-TEM analysis

The HR-TEM analysis, as shown in Fig. 3, was performed to provide evidence for the morphology of the $Zn_{0.6}Mn_{0.4}Fe_2O_4$/PUF nanocomposite. The embedded ferrite nanoparticles were found to be scattered and/or agglomerated together within the PUF. Although agglomerations were inevitable due to the magnetic nature of the ferrite nanoparticles, the polymer foaming reaction reduced dense agglomeration. The average particle size of the nanoparticles within the polymeric nanocomposite varied between 5.3 and 18.5 nm.

3.1.4. SEM analysis

The morphological microstructure of the prepared $Zn_{0.6}Mn_{0.4}Fe_2O_4$/PUF nanocomposite was investigated using SEM analysis. As depicted in Fig. 4A, the prepared nanocomposite's microstructure has a spongy structure of the spherical shape, and the nanoparticles, which appeared as white spots, were homogenously dispersed within the PUF polymer. Furthermore, two forms of pores with different sizes were discovered in the $Zn_{0.6}Mn_{0.4}Fe_2O_4$/PUF nanocomposite, coarse pores ranging in size from 1,240 to 551 μm and medium pores ranging from 199.7 to 121.7 μm. After Cu adsorption, the size of the nanoparticle aggregates increased (Fig. 4B and C), which could be due to adsorbed Cu stuffing into the pores of the nanoparticles [46]. Furthermore, surface roughness and heterogeneity have increased, and a portion of the hexagonal cellular structure has been disrupted. Unlike the use of dewatering agents to activate the surface and increase the porosity of the adsorbent [47], the addition of nanoparticles to PUF had no effect on the cell size of the polymeric nanocomposite.

3.1.5. BET surface area and porosity

In terms of adsorption capabilities, the nanocomposite's surface area is critical. Changes in surface area and pore properties are influenced by a variety of factors, including the initial material and its structure, the activation method chosen, and the agents used. The multipoint BET was used to measure the BET surface area of the $Zn_{0.6}Mn_{0.4}Fe_2O_4$/PUF before and after Cu adsorption from a 2.0 mg L^{-1} solution. The composite material had a specific surface area of 3.202 $m^2\ g^{-1}$ before Cu adsorption and exhibited a Type IV adsorption–desorption isotherm, which is typical of mesoporous materials [48]. $Zn_{0.6}Mn_{0.4}Fe_2O_4$/PUF had a BET surface area of 3.202 $m^2\ g^{-1}$, a pore volume (pores less than 19.858 Å diameter), and an average pore diameter D_p ($4V_{\text{total}}/S_{\text{BET}}$) of $9.38 \times 10^{-3}\ cm^3\ g^{-1}$, and an average pore diameter D_p ($4V_{\text{total}}/S_{\text{BET}}$) of 1.17 nm. They were 2.788 $m^2\ g^{-1}$, $7.89 \times 10^{-3}\ cm^3\ g^{-1}$, and 1.13 nm after Cu adsorption, respectively. Obviously, the surface area of the aggregates has been reduced following Cu adsorption due to filling micropores in the embedded nanoparticles and blocking of the surface of the aggregates as also demonstrated in SEM photographs (Fig. 4C).

3.1.6. Magnetic properties of the nanocomposite

Using a vibrating sample magnetometer at room temperature, the hysteresis loops and the magnetic parameters

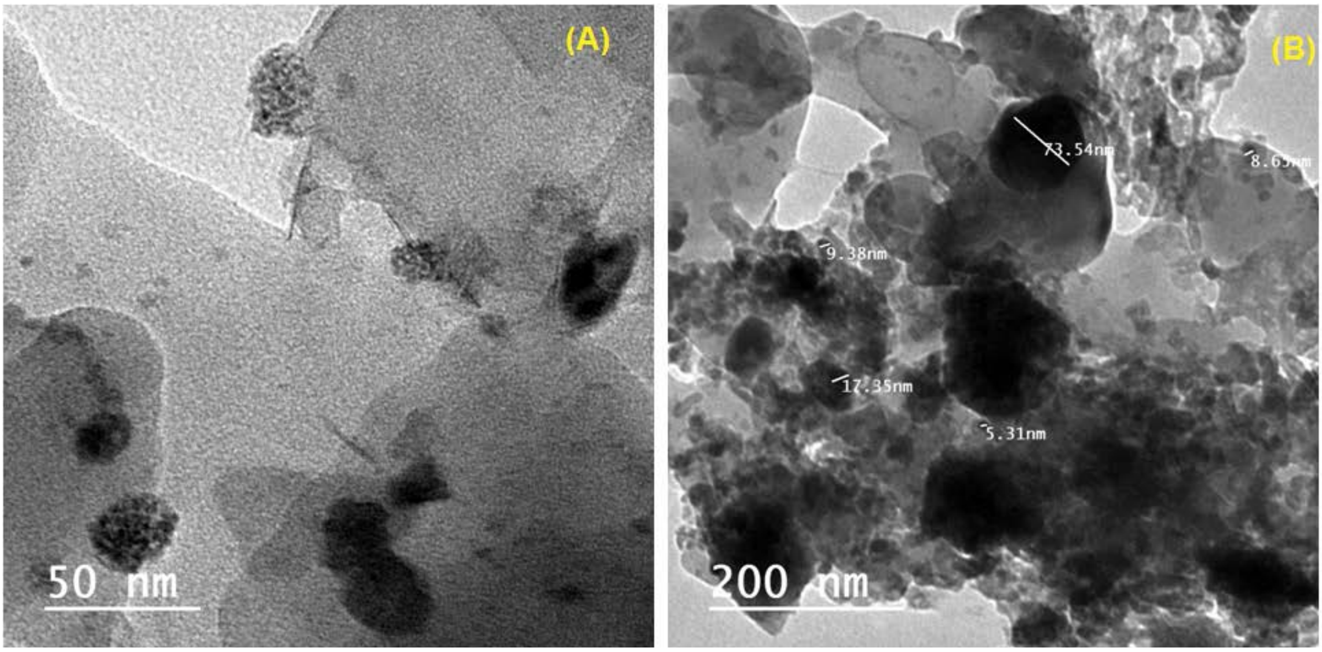

Fig. 3. HR-TEM analysis of the $Zn_{0.6}Mn_{0.4}Fe_2O_4$/PUF polymeric nanocomposite material at 50 nm (A) and 200 nm (B) scales.

such as saturation magnetization (M_s), remanent magnetization (M_r), and coercively (H_c) of the prepared ferrite nanoparticles fired at 400°C for 1 h were measured (Fig. 5). The saturation magnetization and remanent magnetization of the fired sample are 6.6 and 1.7 emu g^{-1}, respectively. In zinc ferrite nanoparticles ($ZnFe_2O_4$), as Zn(II) ions are substituted by Mn(II) ions, the magnetic Mn(II) tends to occupy the A-site in $Zn_{0.6}Mn_{0.4}Fe_2O_4$, reducing the amount of Fe(III) ions at this site. As a result of antiferromagnetic coupling, the net effect is an increase in magnetic activity in site *B*, resulting in enhanced magnetic interactions. The ferromagnetic behavior of $Zn_{0.6}Mn_{0.4}Fe_2O_4$ nanoparticles was also observed, with a coercively value of 216.2G.

3.2. Adsorption study

3.2.1. Sample pH

The pH of the aqueous solution is an important parameter that controls the sorption process because it influences not only the speciation of the metal ion but also the charges on the active adsorption sites. So, the effect of solution pH on the adsorption of Cu and Cd ions onto the proposed nanosorbent $Zn_{0.6}Mn_{0.4}Fe_2O_4$/PUF was studied over a pH range of 2.0–8.0. The results obtained are plotted in Fig. 6A. The adsorption (%) increased gradually with increasing the solution pH from 2.0 to 5.0 and from 2.0 to 6.0 for Cu and Cd, respectively. Beyond these limits,

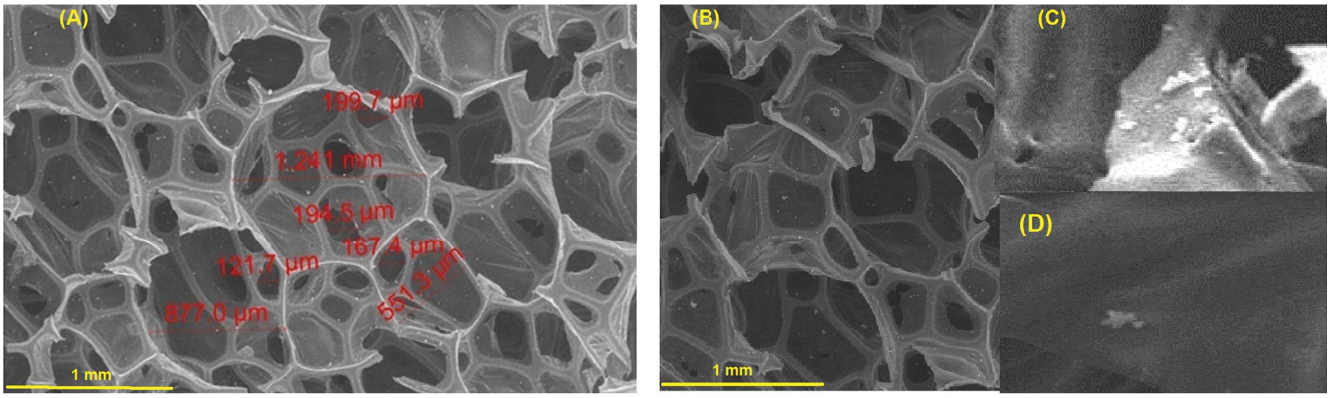

Fig. 4. SEM micrographs of the $Zn_{0.6}Mn_{0.4}Fe_2O_4$/PUF polymeric nanocomposite material before adsorption (A), Cu(II)-loaded nanocomposite (B), and with (C and D) magnified stuffing Cu ions into the nanoparticles.

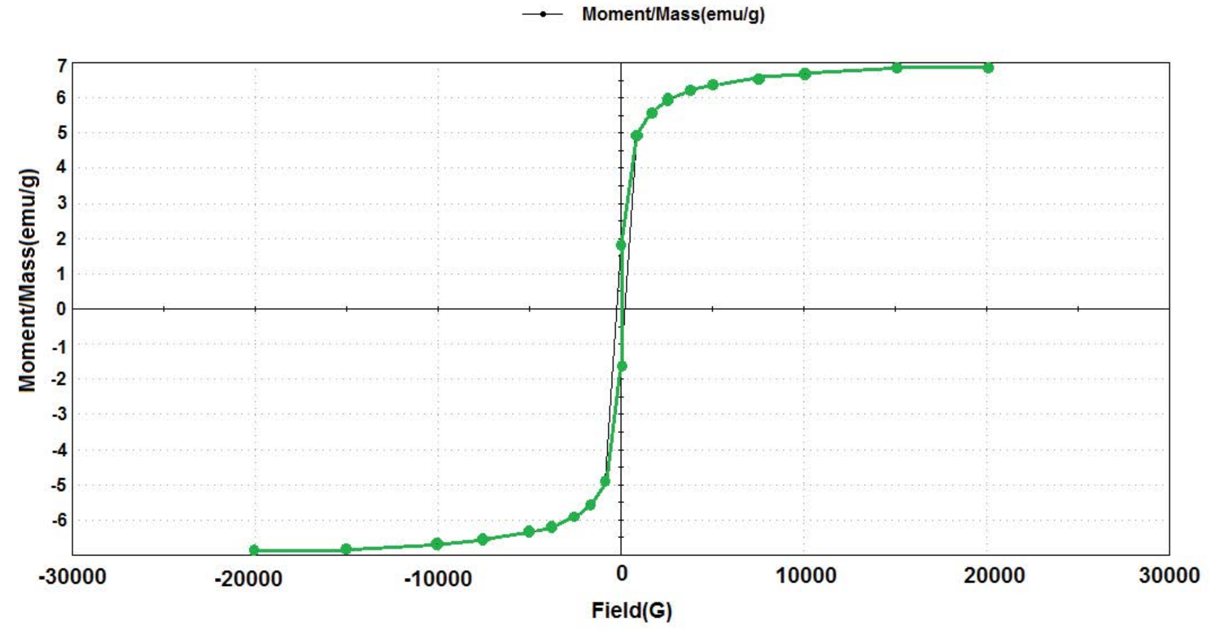

```
Area-1st Quad.: 3595.8 erg/g       Area-2nd Quad.: 550.88 erg/g       Area-3rd Quad.: 3758.8 erg/g
Area-4th Quad.: 511.31 erg/g       Area-Total: 8416.7 erg/g           Coercivity (Hci): 216.15 G
Initial Slope: 1.7266E-6 emu/(g G Magnetization (Ms): 6.8852 emu/g  Mass: 52.000E-3 g
Retentivity (Mr): 1.7190 emu/g     Slope at Hc: 8.0502E-3 emu/(g G)   Squareness: 0.24967
Start Temperature:  0 K            Time Constant: 0.10000 sec
```

Fig. 5. The hysteresis loops and the magnetic parameters of the $Zn_{0.6}Mn_{0.4}Fe_2O_4$ nanoparticles.

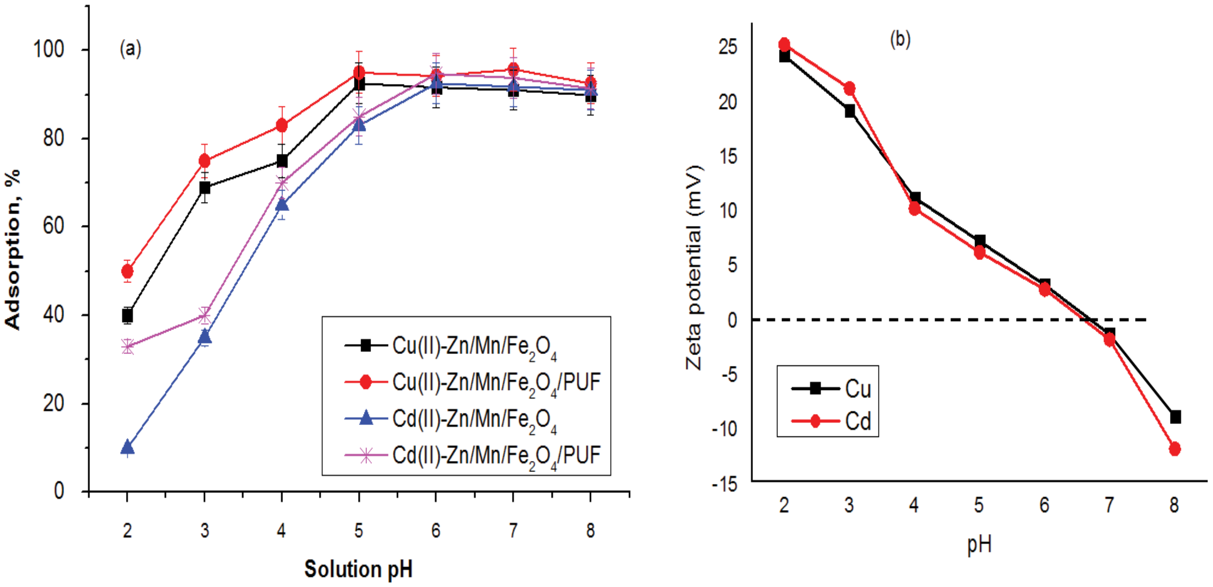

Fig. 6. (a) Effect of pH on the adsorption of Cu and Cd onto $Zn_{0.6}Mn_{0.4}Fe_2O_4$ nanoparticles and $Zn_{0.6}Mn_{0.4}Fe_2O_4$/PUF polymeric nanocomposite at metal ion concentration of 0.8 mg L^{-1}, sample volume 25 mL, sorbent amount of 0.2 g and shaking time of 60 min. (b) Zeta potential of the nanocomposite surface variation with solution pH.

a similar trend for both elements was observed, and the adsorption (%) became maximum and approximately constant up to pH 8.0. The maximum adsorption reached 95% and 94%, respectively. The high adsorption (%) achieved at pH ≥ 6.0 could be attributed to an increase in negatively oxide moieties in the embedded nanoparticles in the adsorbent, which facilitates the attraction of positively charged metal ions [49]. Adsorption ranged from 95%–93% for Cu and 93%–91% for Cd at a pH value ranging from 7.0–8.0, which is similar to the pH range of the studied samples, which is 7.5–8.2 (Table 1), confirming the practical applicability of these water sources. As pH exceeded 8.0, the adsorption decreased slightly. This might be attributed to the possible precipitation of metal hydroxides. At lower pH values than 2.0, there was a significant decrease in the adsorption (%), which could be attributed to protonated active sites repelling positively charged metal ions. However, the nanocomposite adsorbent demonstrated a greater affinity for Cu than Cd at all adsorption stages. Although the difference is around 1.0%, it will become significant and evident when the initial sample concentration increases. The difference in the adsorption affinity may be due to the smaller ionic size of Cu than Cd, which promotes easier diffusion of the former towards the active sites in the sorbent than the latter. Without PUF, the nanoparticles $Zn_{0.6}Mn_{0.4}Fe_2O_4$ showed similar pH profiles, but their adsorption was always lower than that of $Zn_{0.6}Mn_{0.4}Fe_2O_4$/PUF. The maximum adsorption obtained was 93% for Cu or Cd. Thus, pH 6.5 was recommended as the optimum value in all subsequent adsorption studies of the two elements. It is worth mentioning that untreated PUF has no ability to adsorb Cu and Cd ions unless chelating agents, for example, thiocyanate, are present [50]. Therefore, the role of PUF is expected to be limited to carrying the adsorbent. However, we noticed that the presence of PUF improved the efficiency of the adsorbent even at low pH values. This could be due to the PUF helping to distribute the nanoparticles over a larger surface area of the nanocomposite. As a result, the surface area exposed to adsorption grew. The nanocomposite's point of zero-electric charge (pH_{PZC}) was determined at pH 6.8, as illustrated in Fig. 6B. Positive potential for the nanocomposite was obtained at pH ranging from 2.0 to 6.0 due to protonated surface groups of the nanoparticles and PUF. As pH increased, Cu and Cd became positively charged free ions Cu^{2+} and Cd^{2+}, as well as the monohydroxylated species $Cu(OH)^+$ and $Cd(OH)^+$. With increasing pH, the potential dropped due to deporotonation of the nanocomposite surface groups and the liberation of negatively charged sites, which helped adsorption by electrostatic attraction mechanism. When the pH hit 6.8, negative charges on the adsorbent surface were totally neutralized. Beyond pH 6.8, the potential was negative, indicating that there was no electrostatic attraction and that adsorption was based on metal hydroxide precipitation. Moreover, in ferrite OH groups, metal ions may also substitute hydrogen atoms, resulting in the creation of negatively charged oxygenates on the nanocomposite [8].

3.2.2. Adsorption kinetics

The effect of time on adsorption determines the possibility of using the new nanocomposite for the rate at which the metal ions transfer from the aqueous phase to the solid sorbent. The shaking time was studied over a range of 1–75 min. Results obtained for the variation of the adsorbed amount q_t (mg g^{-1}) at any time t is shown in Fig. 7. During the first 5 min, the uptake was very rapid, and more than 50% of the adsorbed amount was achieved after 1 min. Beyond 10 min, the adsorption increased at a slower rate, reaching the equilibration state and maximum

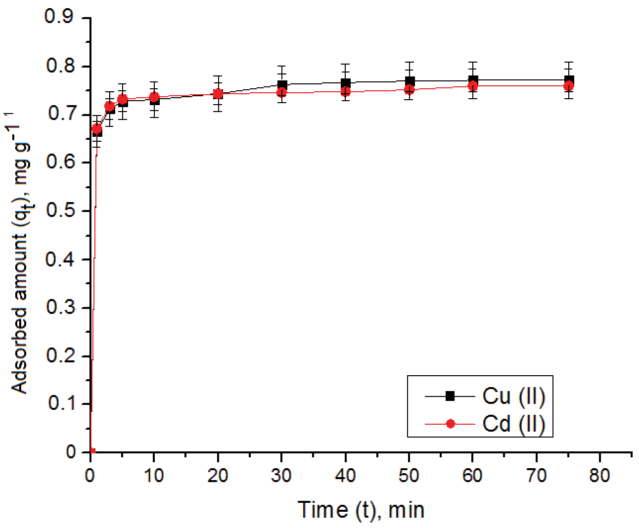

Fig. 7. Effect of shaking time on the adsorption of Cu and Cd onto $Zn_{0.6}Mn_{0.4}Fe_2O_4$/PUF polymeric nanocomposite at metal ion concentration of 0.8 mg L^{-1}, sample volume 25 mL and sorbent amount of 0.2 g.

adsorption after 40 and 60 min for Cu and Cd, respectively. The early rapid adsorption demonstrates the accessibility of the $Zn_{0.6}Mn_{0.4}Fe_2O_4$/PUF composite material for removing Cu and Cd ions from an aqueous solution. This also confirms the high binding constant between the metal ions and the composite material, implying that it is relevant for the selective removal of these elements from interfering matrices. Finally, in the subsequent experiments, the shaking time was selected at 60 min to emphasize quantitative adsorption and achieve equilibration conditions.

The kinetic mechanism governing metal ion adsorption was studied by fitting experimental results to the pseudo-first-order, pseudo-second-order, and intraparticle diffusion models. The validity of the pseudo-first-order model could be examined by plotting $\log(q_e - q_t)$ vs. t, where q_e and q_t represent the adsorbed amount of metal ion (µg g^{-1}) at equilibrium and at any time t (min), respectively. The Lagergren and Kungliga [51] pseudo-first-order rate is expressed by Eq. (5):

$$\log(q_e - q) = \frac{\log q_e - k_1 t}{2.303} \tag{5}$$

As shown in Table 2, the regression analysis results show linear correlation coefficients (R^2) of 0.930 and 0.759 for Cu and Cd, respectively, and q_e values of 1.49 and 2.01 mg g^{-1}. A very significant discrepancy was found with the experimental q_e values of 0.78 and 0.77 mg g^{-1}, respectively, showing that the pseudo-first-order model is inconvenient for describing the adsorption kinetics results.

The pseudo-second-order suggested by Ho et al. [52] is expressed by Eq. (6):

$$\frac{t}{q_t} = \frac{1}{\left(k_2 q_e^{\,2}\right)} + \left(\frac{1}{q_e}\right) t \tag{6}$$

where k_2 is the pseudo-second-order rate constant (µg g^{-1} min^{-1}). Fig. 8 depicts a plot of the experimental results with this model. The R^2 values obtained from the slope of the regression equations are greater than those derived from the pseudo-first-order model, with values of 0.999 and 0.999. Furthermore, the calculated q_e values from the second-order model were remarkably similar to experimental results. This verified that the pseudo-second-order model is appropriate for investigating the experimental kinetic effects.

The Morris–Weber Eq. (7) was used to investigate the intraparticle diffusion behavior [53]. The slope of the plot of q_t values vs. the square root of shaking time t was used to evaluate the intraparticle diffusion rate constant k_{id} (mg g^{-1} $min^{-1/2}$).

$$q_t = k_{id} t^{1/2} \tag{7}$$

The plots for the two elements revealed a linear relationship with higher slopes at early time intervals, followed by a second linear range with lower slopes, suggesting a multistep adsorption mechanism. The straight lines did not pass through the origin, indicating that a film diffusion phase occurred during the initial adsorption stages and intraparticle diffusion contributes to the rate-limiting step, as can be seen in Fig. 8B. The calculated R^2 values were 0.957 and 0.962 for Cu and Cd, respectively, and k_{id} values of 0.085 and 0.081 mg g^{-1} $min^{-1/2}$. PUF is a highly porous material that has spherical and symmetrical macropores and micropores. The macropores are large in comparison to the molecular size of the solute and easily accessible to metal ions. Therefore, adsorption into the macropores occurs quickly, as is typical of film diffusion. The micropores, on the other hand, are around the same size as the metal ion, and diffusion inside these pores will be seriously hampered due to steric hindrances. As a consequence, an intraparticle diffusion mechanism will have a slow approach to equilibrium. Thus, intraparticle diffusion in the microporous regions of the sorbent governed

Table 2
Adsorption kinetic data obtained from pseudo-first-order, pseudo-second-order and intraparticle diffusion models at 25°C

Metal ion	q_{exp}, mg g^{-1}	Pseudo-first-order			Pseudo-second-order			Intraparticle diffusion	
		q_e, mg g^{-1}	k_1, min^{-1}	R^2	q_e, mg g^{-1}	k_2, mg g^{-1} min^{-1}	R^2	k_{id}, mg g^{-1} $min^{-1/2}$	R^2
Cu(II)	0.77	1.49	0.046	0.930	0.78	3.02	0.999	0.085	0.975
Cd(II)	0.75	2.01	0.037	0.759	0.77	4.05	0.999	0.081	0.962

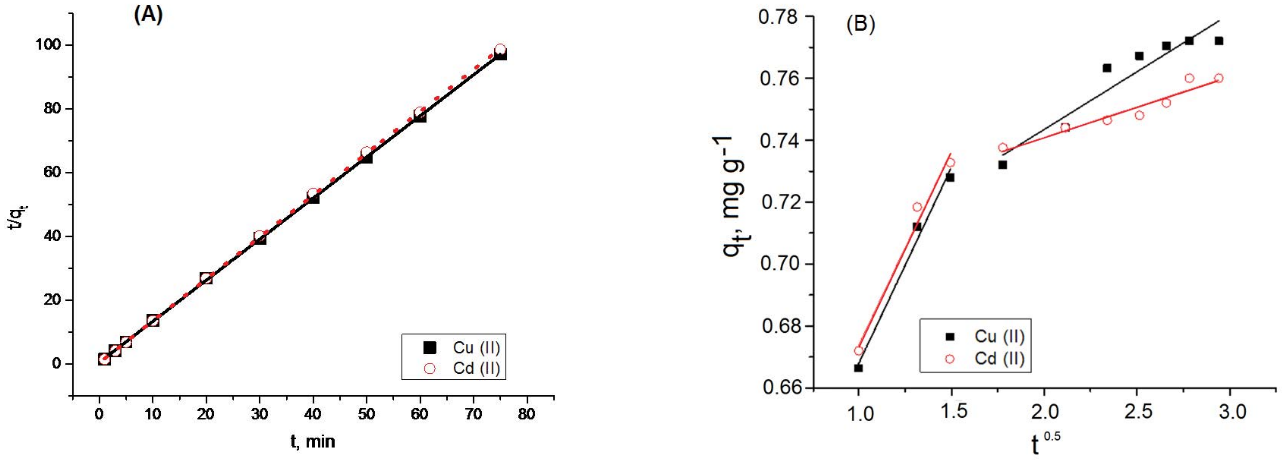

Fig. 8. Pseudo-second-order kinetic (A) and intraparticle diffusion (B) models of the adsorption of Cu and Cd onto $Zn_{0.6}Mn_{0.4}Fe_2O_4$/PUF polymeric nanocomposite at metal ion concentration of 800 μg L^{-1}, sample volume 25 mL and adsorbent amount of 0.2 g.

the bulk sorption of metal ions. The transfer of metal ions into the polymeric material's narrow apertures greatly increases the rate of accumulation of these ions in the solid phase, allowing for a faster rate of adsorption.

As a result, the metal kinetic adsorption process into the $Zn_{0.6}Mn_{0.4}Fe_2O_4$/PUF composite adopted the diffusion-controlled and pseudo-second-order kinetic models. The goal of using PUF as a nanoparticle carrier is to take advantage of its large surface area, which makes the nanoparticles embedded more susceptible to metal ion interference. This speeds up the rate of mass transfer and diffusion, making the adsorption process go much faster. Furthermore, the polymer swells to a cellular structure during the foaming process, where the hydrophilic terminal groups of PUF interact with the added metallic oxides, reducing the dense agglomeration of the magnetic nanoparticles.

3.2.3. Adsorption isotherm

Adsorption isotherm study enables to evaluate the equilibrium adsorption capacity and the metal nanocomposite binding strength. The Langmuir, Freundlich and Temkin isotherm models were examined to fit the experimental results. Langmuir isotherm [54] is expressed by Eq. (8).

$$\frac{C_e}{q_e}=\frac{C_e}{q_{\max}}+\frac{1}{q_{\max}K_L} \tag{8}$$

where $q_{\max}$ is the maximum adsorbed amount of metal ion (mg g^{-1}) to form a complete monolayer. C_e is the equilibrium concentration of the metal ion (mg L^{-1}) and K_L is the Langmuir constant related to the affinity of binding sites to metal ions. This model, if matched with the experimental results, assumes a monolayer adsorption mechanism. The maximum monolayer adsorption capacity ($q_{\max}$, mg g^{-1}) was calculated from this model.

Freundlich isotherm [55] is an empirical model based on adsorption on heterogeneous surfaces, as presented by Eq. (9).

$$\ln q_e=\left(\frac{1}{n}\right)\ln C_e+\ln K_F \tag{9}$$

where q_e is the adsorbed amount of metal ion (mg g^{-1}), C_e is the equilibrium concentration of the metal ion (mg L^{-1}), and K_F and n are Freundlich constants related to adsorption capacity and intensity, respectively.

The Temkin isotherm model [56] described by Eq. (10) was applied to describe and evaluate the heat of adsorption and the adsorbent–adsorbate interaction.

$$q_e = B\ \ln A_T + B\ \ln C_e \tag{10}$$

where A_T is the Temkin isotherm equilibrium binding constant (L g^{-1}) and B is the heat of adsorption (J mol^{-1}).

Based on the slightly higher correlation coefficients than the Langmuir model, the Freundlich isotherm model was more fitting to describe the adsorption behavior which indicates the importance of surface heterogeneity, as shown in Fig. 9 and Table 3. These findings imply that the adsorption process can progress by forming multilayer coverage at the adsorbent interface. This also accounted for surface heterogeneity and provided an exponential distribution of energetic active sites on the adsorbent surface. This is consistent with the presence of coarse and medium pores in the SEM micrographs of the nanocomposite sorbent. Adsorption process may begin with the metal ion diffusion from the bulk of the solution to the sorbent surface, then to the inner surface to combine with active groups for ultimate accumulation in a monolayer or extended to a multilayer pattern.

The calculated maximum capacity ($q_{\max}$) from the Langmuir model was found to be 20.4 and 11.1 mg g^{-1}, respectively. The large difference in adsorption capacity can be due to differences in ionic size, the binding strength with the nanocomposite, and degree of hydration [57]. Because Cu has a greater capacity than Cd, the chelating sites are more accessible to Cu.

The Freundlich constant K_F was 0.62 (Cu) and 0.31 (Cd) L g^{-1} which shows a stronger affinity of the sorbent towards

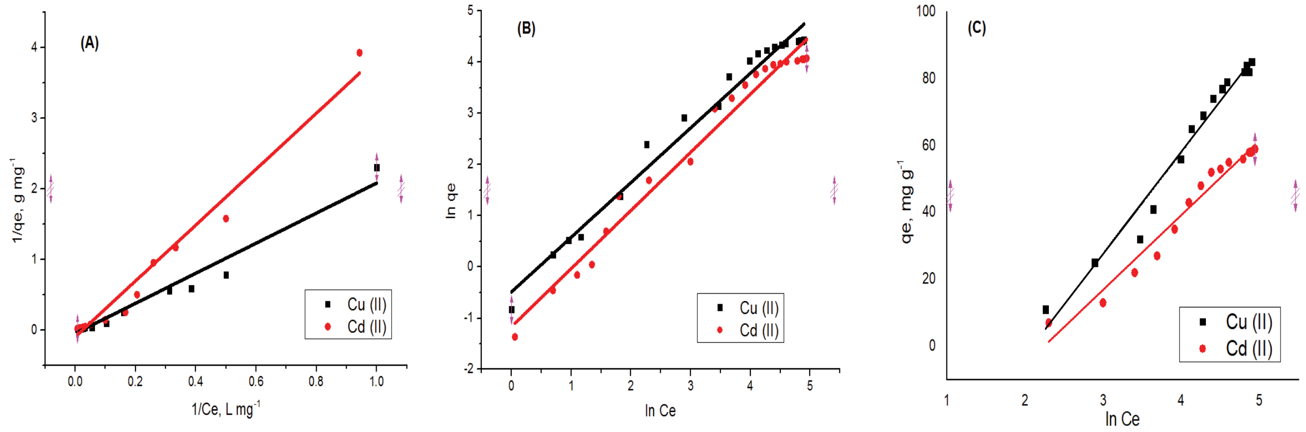

Fig. 9. Langmuir (B), Freundlich (B), and Temkin (C) isotherm models of the adsorption of Cu and Cd onto $Zn_{0.6}Mn_{0.4}Fe_2O_4$/PUF polymeric nanocomposite at initial metal ion concentration from 0.2 to 300 mg L^{-1}, pH 6.5, sample volume 25 mL, adsorbent amount of 0.2 g, and shaking time of 60 min.

Cu than Cd. The value of the n constant was 0.93 (Cu) and 0.88 (Cd) which is adequate for favorable adsorption. The value of n is slightly lower than one, indicating a cooperative adsorption and the adsorbent has a higher adsorption affinity towards the tested metal ions. The values of both constants indicated the feasible adsorption of these metal ions by the developed nanocomposite. The Temkin isotherm model showed good correlation by avoiding the lower concentrations. The R^2 value was 0.969 and 0.963. Also, the constant A_T was 2.07 and 2.24 L g^{-1} and the constant B was 30.4 and 22.3 J mol^{-1}, respectively. Also, the positive B values indicated the adsorption is an exothermic process.

3.3. Competitive adsorption

The competitive adsorption of Cu and Cd can be explained using kinetic and adsorption capacity results. Within the first 10 min the adsorption of these metal ions followed a fairly similar pattern, according to a kinetic profile (Fig. 7). A pseudo-second-order kinetic model depicted the adsorption, which is characteristic of a regulated stage of chemical adsorption. The overall adsorption rate constant k_2 was 0.014 and 0.017 g g^{-1} min^{-1} for Cu(II) and Cd(II), respectively. In addition, Cu has a higher Langmuir monolayer adsorption capacity and Freundlich affinity constants (k, n) than Cd, as shown by the isotherm features in Table 3. As a result, Cu adsorption is projected to occur first and with a stronger affinity when the two elements are mixed, resulting in less Cd adsorption. In the microporous area, the two metal ions displayed identical intraparticle diffusion (k_{id}). Consequently, ferrite nanoparticles could be the main cause. In spinel ferrites, there are several types of adsorption centers (Fe–OH, Zn–OH, and Mn–OH) with varied affinities to metal ions [58]. A probable explanation is a difference in ionic size, with Cd being larger than Cu. Various types of adsorption centers appear to have been filled during Cu adsorption, however, only a few types of these sites are appropriate for Cd adsorption.

Table 3
Isotherm parameters obtained from Langmuir, Freundlich, and Temkin models

Isotherm model	Parameters	Cu	Cd
Langmuir	q_{max}, mg g^{-1}	20.4	11.1
	K_L, L mg^{-1}	0.03	0.02
	R^2	0.962	0.970
Freundlich	n	0.93	0.88
	K_F	0.62	0.31
	R^2	0.988	0.980
Temkin	B_T (J mol^{-1})	30.4	22.3
	b_t	81.5	111.1
	A_T, L g^{-1}	2.07	2.24
	R^2	0.969	0.963

3.4. Adsorption mechanism

A variety of factors influence metal adsorption, including metal shape, size, and structure; adsorbent textural properties and surface chemistry; and the specific interaction between the adsorbent surface and metal ions [47]. The proposed adsorption mechanism is demonstrated in Fig. 10. The solution pH is strongly related to the adsorption mechanism, which determines the metal ion species and the ionization of the nanocomposite's functional groups. Results showed maximum adsorption occurred at pH 6.0–7.0 where Cu and Cd exist as Cu^{2+}, $Cu(OH)^+$ and Cd^{2+}, $Cd(OH)^+$ forms, respectively with a greater amount as $Cu(OH)^+$ and $Cd(OH)^+$ species [49]. Electrostatic attraction to negatively charged oxide groups in the nanocomposite allows the $M(OH)^+$ species (M stands for Cu and Cd) to be adsorbed to one negative charge as $Zn_{0.6}Mn_{0.4}Fe_2O_4$-O-MOH. Adsorption of $M(OH)^+$ species facilities the conversion of Cu^{2+} and Cd^{2+} into the easily adsorbed forms $Cu(OH)^+$ and $Cd(OH)^+$. Ion exchange adsorption could occur by substituting the H^+ in $Zn_{0.6}Mn_{0.4}Fe_2O_4$-OH to form $Zn_{0.6}Mn_{0.4}Fe_2O_4$-O-MOH. This is explained by the

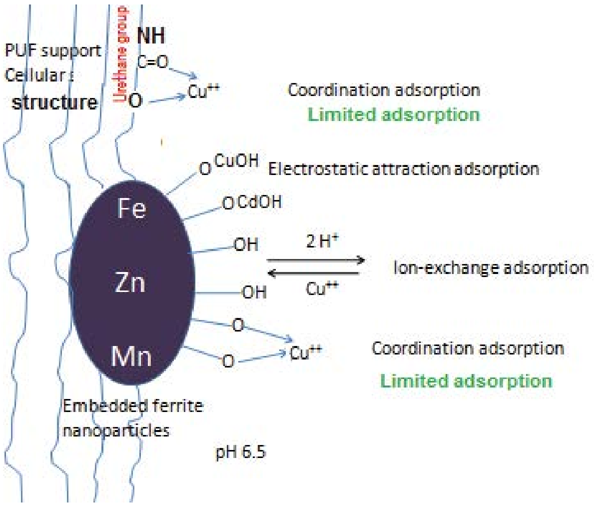

Fig. 10. Proposed adsorption mechanisms of the studied metal ions (e.g., Cu) onto the nanocomposite surface groups.

extremely short equilibration time (10 min) that accounts for electrostatic attraction and ion exchange adsorption (Fig. 7). Adsorption by precipitation is excluded because the $Cu(OH)_2$ and $Cd(OH)_2$ would form at pH levels greater than 7.4 and 8.0, respectively. The adsorption isotherm followed the Freundlich model, indicating the surface heterogeneity of the nanocomposite adsorbent made of ferrite and PUF materials, but the nanoparticles embedded were mostly regulated.

Form the FT-IR data, despite the urethane carbonyl (C=O) groups being shown in the FT-IR spectra to be involved in coordination with the investigated elements, the extent of this type of adsorption is relatively limited in the absence of complexing agents [59]. The results also indicate that metal ions are directly coordinated in the nanocomposite within the foam phase by using donor atoms in the nanoparticles [60,61]. As a result, metal ion removal occurs through heterogeneous chemisorption mechanism.

3.5. Nanocomposite dosage

The composite dosage has an important impact on metal ion adsorption from aqueous solutions. The effect of $Zn_{0.6}Mn_{0.4}Fe_2O_4$/PUF weight on adsorption was investigated from 0.025 to 0.3 g using 25 mL samples and a metal ion concentration of 0.8 mg L^{-1}. The results obtained are shown in Fig. 11. The adsorption (%) increased steadily as the weight increased from 0.025 to 0.2 g. At a weight of 0.2 g, maximum adsorption for Cu(II) and Cd(II) was 96% and 98%, respectively. This may be due to the higher adsorbent amount, which increases the number of active sites available for adsorption, resulting in more efficient metal ion removal [62]. Beyond this limit, as the amount of sorbent was increased, the adsorption (%) remained significantly unchanged. This behavior suggests that, after a certain dosage, the optimum adsorption is reached, and thus the remaining concentration of metal ions stays constant even as the dosage is increased. Perhaps a higher composite amount may prevent metal ions from accessing the available adsorption sites. Finally, a composite weight of 0.2 g was recommended in the subsequent investigations.

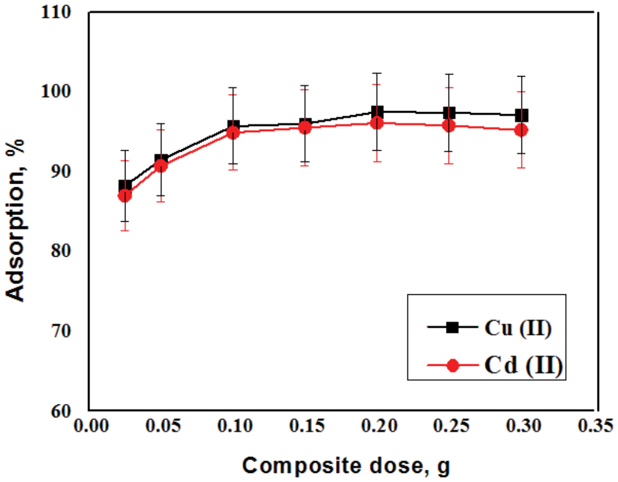

Fig. 11. Effect of composite dosage on the adsorption of Cu and Cd by $Zn_{0.6}Mn_{0.4}Fe_2O_4$/PUF polymeric at metal ion concentration of 0.8 mg L^{-1}, sample pH 6.5 and volume of 25 mL, and shaking time of 60 min.

Fig. 12 depicts the effect of initial metal ion concentration on adsorption efficiency and uptake at various composite dosages within the range from 0.5 to 3.0 mg L^{-1}, and the composite dosage was investigated at 0.05, 0.1, 0.2, and 0.3 g. The uptake of Cu and Cd was found to increase gradually and closely at initial concentrations up to 1.0 mg L^{-1}. Following that the difference in uptake gradually increased with Cu outperforming Cd. The adsorption efficiency (%) was highly dependent on the initial metal ion concentration. The adsorption efficiency (%) for Cu and Cd decreased from 99% to 87% and from 95% to 63%, respectively, for Cu and Cd by increasing the concentration from 0.5 to 3.0 mg L^{-1}. The decrease for Cu was less than 12%, whereas the decrease for Cd was 32%, indicating that Cu adsorption is less dependent on the initial concentration than Cd. The gradual decrease in adsorption with increasing initial concentration can be attributed to increasing the metal ion concentration above the adsorbent capacity, which causes the remained concentration of metal ions to gradually increase, and thus the adsorption efficiency decreases. The effect of the composite dose on the uptake and adsorption efficiency revealed very similar profiles (Fig. 12B). They increased by increasing the sorbent dose up to 0.2 g, and then decreased slightly when they reached 0.3 g. Maximum uptake and adsorption efficiency were obtained. When the adsorbent dose was increased from 0.05 to 0.1 g, the Cd uptake increased by 0.14 mg g^{-1} and by 0.2 mg g^{-1} when the sorbent dose was increased from 0.1 to 0.2 g.

3.6. Interference effect

The adsorption of the studied metal ions was investigated in the presence of a foreign ion such as Na^+ (10,000 mg L^{-1}), K^+ (1000 mg L^{-1}), Ca^{2+} (500 mg L^{-1}), Mg^{2+} (100 mg L^{-1}), Zn^{2+} (1.0 mg L^{-1}), Ni^{2+} (1.0 mg L^{-1}),

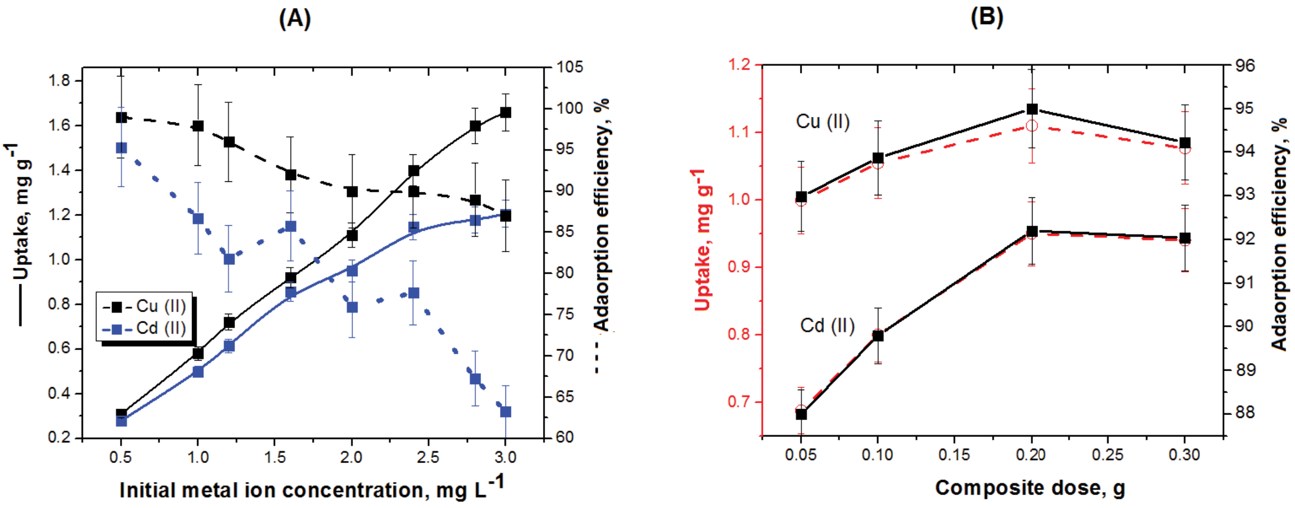

Fig. 12. Influence of initial metal ion concentration (A) and nanocomposite dosage (B) on uptake and adsorption efficiency: initial concentration varied from 0.5 to 3.0 mg L^{-1} using a composite dose of 0.2 g. The adsorbent dosage varied from 0.05 to 0.3 g at an initial metal ion concentration of 2.0 mg L^{-1}, at a sample pH of 6.5, sample volume of 25 mL, and shaking time of 60 min.

Cl^- (10,000 mg L^{-1}), SO_4^{2-} (500 mg L^{-1}), PO_4^{3-} (50 mg L^{-1}), NO_3^- (100 mg L^{-1}), or oxalate (50 mg L^{-1}). Synthetic solutions containing Cu or Cd (0.8 mg L^{-1}), as well as the foreign ion, were prepared and adjusted to the best adsorption conditions. The recovery (%) of the metal ion studied was compared to that obtained in the absence of the foreign species. The addition of foreign ions had no significant influence on recovery (%), with the largest decreases for Cu and Cd being no more than –3.7% and –4.5%, respectively (Fig. 13). This demonstrated the produced sorbent is suitable for the adsorption/removal of the tested elements from natural water because of its selective adsorption even in the presence of many folds of the interfering ions.

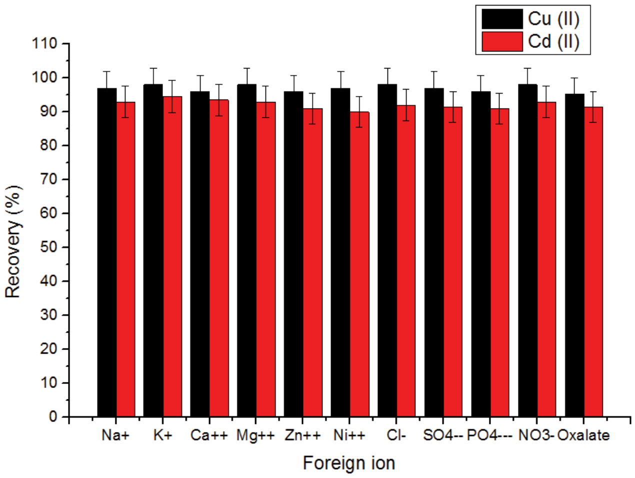

Fig. 13. Influence of interfering ions on the recovery (%) of Cu or Cd each at a concentration of 0.8 mg L^{-1}, adsorbent dosage of 0.2 g, pH 6.5, sample volume 25 mL, and shaking time of 60 min.

3.7. Preconcentration and recovery

In the case of contaminated waters or low metal ion concentrations, a preconcentration/separation step is required to allow FAAS to detect the element accurately. The ability of the developed adsorbent to preconcentrate low concentrations of metal ions from large sample volumes justifies its feasibility. For this purpose, the sample volume was varied from 50 to 1,500 mL, with a fixed amount of 20 µg metal ion, pH adjusted to 6.5, an adsorbent amount of 0.2 g, and a shaking period of 60 min. The results are summarized in Table 4. When the volume was increased from 50 to 1,250 mL, the recovery (%) for Cu and Cd decreased from 95% to 92% and from 95% to 94%, respectively, corresponding to a drop in metal ion concentration from 400 to 16 µg L^{-1}. Beyond this volume, the recovery was ≤90%, and the preconcentration was deemed non-significant. Therefore, 1,250 mL was estimated as the breakthrough volume and the limit of preconcentration. The quantitative recovery limit was set at the breakthrough volume, which was within ±5.0% deviation of the initial recovery. The estimated sample breakthrough volume for quantitative recovery of the elements was utilized to calculate the preconcentration factor (CF) by dividing the sample volume by the eluate volume. Under the optimal sorption–desorption conditions, the added 20 µg of metal ion could be quantitatively recovered using 10 mL of the eluent without substantial analyte loss. Thus, the CF for each metal ion is estimated to be 125. The limit of quantification (LOQ) was evaluated as ten times the standard deviation of the blank signal (10 σ) obtained using the sorption–desorption method with 25 mL of blank solution ($n = 4$). The LOQ values for Cu and Cd were determined to be 0.9 and 1.4 µg L^{-1}, respectively.

3.8. Reusability

To estimate the reusability of the proposed sorbent $Zn_{0.6}Mn_{0.4}Fe_2O_4$/PUF, a sorption–desorption study was

Table 4
Preconcentration, recovery (%) and preconcentration factor (CF) of Cu and Cd using $Zn_{0.6}Mn_{0.4}Fe_2O_4$/PUF composite sorbent and final volume of HCl eluent (0.5 mol L^{-1}, 10 mL)

Element	Sample volume, mL	Concentration added in sample, µg L^{-1}	Concentration found in eluent ± S.D. (n = 3), µg L^{-1}	Recovery, %	CF
Cu(II)	50	400	380.0 ± 10.3	95	5
	100	200	189.0 ± 5.5	95	10
	250	80	75.4 ± 5.0	94	25
	500	40	37.6 ± 2.7	94	50
	1,000	20	18.8 ± 1.0	94	100
	1,250	16	14.7 ± 0.5	92	125
	1,500	13	11.5 ± 0.8	89	150
Cd(II)	50	400	381.2 ± 16.0	95	5
	100	200	190.0 ± 14.0	95	10
	250	80	75.9 ± 3.1	95	25
	500	40	37.8 ± 3.5	95	50
	1,000	20	18.8 ± 0.7	94	100
	1,250	16	14.9 ± 1.4	94	125
	1,500	13	11.7 ± 0.9	90	150

carried out for several cycles with Cd at 0.8 mg L^{-1} concentration, 0.2 g adsorbent amount, solution pH of 6.5, a sample volume of 25 mL, and a shaking time of 60 min. After the element was extracted, the Cd-loaded adsorbent was washed with DDW and then treated with 10 mL of 0.5 mol L^{-1} HCl solution as an eluting agent. Following each desorption experiment, the adsorbent was washed several times with DDW until it was acid-free, air dried, and reused for the next cycle. By repeating 7 cycles of successive sorption–desorption experiments with the same adsorbent material, the reusability of the $Zn_{0.6}Mn_{0.4}Fe_2O_4$/PUF composite for Cd adsorption was assessed. The results achieved are shown in Fig. 14A. After 5 cycles, the Cd removal performance of the composite remained almost unchanged, with a 1% decrease in recovery. At higher cycles than 5, a small decrease in recovery (%) was observed, suggesting that the $Zn_{0.6}Mn_{0.4}Fe_2O_4$/PUF composite could maintain its functionality for more than 5 cycles without losing significant adsorptive capability. However, the number of cycles will be increased if a low-concentration eluent is used. This indicates that the $Zn_{0.6}Mn_{0.4}Fe_2O_4$/PUF composite has ample stability and is considered robust for many adsorption–regeneration and reutilization, confirming that the prepared composite materials can be used as a cost-effective adsorbent. For the first seven cycles, the accuracy of Cd recovery was assessed under the optimum conditions for batch sorption–desorption. The average recovery was 93% ± 2.1 with an average deviation of 1.6%. The reusability was calculated using the relative standard deviation (RSD), and the value was 2.2%, indicating good accuracy (less than 10%).

3.9. Leaching effect

The leaching of Fe, Mn, and Zn from nanocomposite embedded nanoparticles was investigated. A 0.2 g composite dose was placed in 25 mL metal-free solutions ranging in pH from 2 to 8 and shaken for 1 h at 25°C. The FAAS technique was used to determine the concentration of the leaked elements. The obtained results are shown in Fig. 14B. The concentrations of Fe, Mn, and Zn ranged from 1.3 to 0.0, 2.2 to 0.0, and 2.0 to 0.0 mg L^{-1}, respectively. At the chosen pH of 6.5 for adsorption, neither element's concentration exceeded 0.05 mg L^{-1}. The presence of several polar groups in PUF polymer that can bind with metal oxide nanoparticles contributed to the adequate nanocomposite stability. This also demonstrated that the developed material is an environmentally friendly adsorbent.

3.10. Applications to real waters

The developed $Zn_{0.6}Mn_{0.4}Fe_2O_4$/PUF nanocomposite was validated for pre-adsorption/removal of Cu and Cd from three water samples obtained from Faiyum Governorate: Qaroun Lake, Yousef River, and tap water. The validity of the method was assessed by applying the standard addition protocol [63] to the new procedure. The added-found assay was performed on 25 mL water samples that had been spiked with 0, 200, and, 400 µg L^{-1} of each metal ion and mixed with 0.2 g of adsorbent. The analysis was carried out in triplicate and the average value of the observed concentration as well as the relative standard deviation (RSD %) were calculated. Results obtained are shown in Table 5. The recovery of Cu ranged from 89%–103%, with the corresponding RSD values of 1.4%–7.3%. For Cd, the recovery varied from 95% to 116%, with the corresponding RSD value ranging from 0.8% to 8.6%. Obviously, the recovery for Cu is relatively low, possibly due to interference with matrix ions in water, whereas Cd recovery is deemed adequate. Despite this, the results are considered relevant for real-samples analysis because the RSD values are less than 10%, indicating good accuracy and precision of the method.

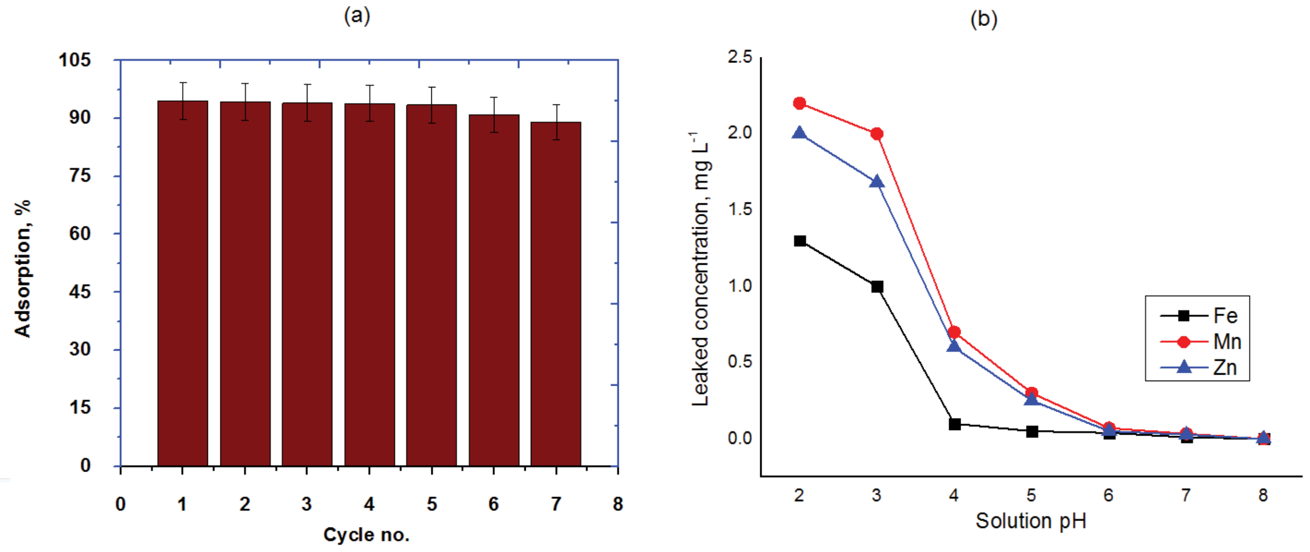

Fig. 14. (a) Reusability of $Zn_{0.6}Mn_{0.4}Fe_2O_4$/PUF nanocomposite for the first seven adsorption–desorption cycles for Cd at a concentration of 0.8 mg L^{-1} at adsorbent dosage 0.2 g, pH 6.5, sample volume 25 mL, and shaking time of 60 min. (b) Leaching of Fe, Mn and Zn from the nanocomposite with variation of solution pH.

Table 5
Recovery data of Cu and Cd for the spiked Qaroun Lake, tap water and Yousef River using $Mn_{0.4}Zn_{0.6}Fe_2O_4$/PUF composite sorbent

Water sample	Metal ion	Added, μg L^{-1}	Found (Mean ± S.D., $n = 3$), μg L^{-1}	Recovery (%)	RSD (%)
Qaroun Lake	Cu(II)	0	47.0 ± 1.5	–	3.2
	Cu(II)	200	225.0 ± 6.0	89	2.7
	Cu(II)	400	410.8 ± 12.0	91	2.9
	Cd(II)	0	7.7 ± 0.4	–	5.2
	Cd(II)	200	233 ± 5.0	113	2.1
	Cd(II)	400	403.0 ± 19.0	99	4.7
Yousef River	Cu(II)	0	45.0 ± 3.3	–	7.3
	Cu(II)	200	229.0 ± 4.0	92	1.7
	Cu(II)	400	457.0 ± 23.0	103	5.0
	Cd(II)	0	6.3 ± 0.28	–	4.4
	Cd(II)	200	238.0 ± 2.0	116	0.8
	Cd(II)	400	391.5 ± 31.0	96	7.9
Tap water	Cu(II)	0	35.0 ± 1.8	–	5.1
	Cu(II)	200	215.0 ± 3.0	90	1.4
	Cu(II)	400	398.0 ± 10.0	91	2.5
	Cd(II)	0	5.0 ± 0.35	–	7.0
	Cd(II)	200	226.0 ± 6.0	111	2.7
	Cd(II)	400	385.4 ± 33.0	95	8.6

4. Comparison to other sorbents

Table 6 compiles a comparison of the adsorption capacity and CF obtained by the $Zn_{0.6}Mn_{0.4}Fe_2O_4$/PUF nanocomposite with other reported sorbents. In view of the adsorption capacity, the developed sorbent outperformed the capacity of many chemically functionalized materials [40,65–70], including the PUF-based sorbents such as alizarin complexone-PUF, carbon disulfide-PUF, 2-aminothiazole, and functionalized polymers such as Alizarin red S XAD-2, and the diacetyl monoxime modified silica gel sorbent. In comparison to other composite sorbents [43,70–76], the present material had a comparable or higher capacity. Indeed, many newly developed adsorbents [8,48,77] had capacities that were several to tens of times higher than those obtained. However, this is primarily dependent on the method of preparation, so increasing the amount of embedded $Zn_{0.6}Mn_{0.4}Fe_2O_4$ nanoparticles in the polymeric

Table 6
Comparison of the adsorption capacity and preconcentration factor (CF) of $Zn_{0.6}Mn_{0.4}Fe_2O_4$/PUF nanocomposite relative to Cu and Cd with other reported materials

Sorbent	Metal ion	Adsorption capacity, mg g^{-1}	CF	References
$Mn_{0.4}Zn_{0.6}Fe_2O_4$/PUF nanocomposite	Cu(II)	20.4	125	This work
	Cd(II)	11.1	125	
Alizarin complexone-PUF	Cu(II)	2.08	100	[40]
	Cd(II)	0.56	100	
Carbon disulfide-PUF	Cu(II)	0.20	100	[64]
2-Aminothiazole-PUF	Cd(II)	0.43	100	[66]
4-Hydroxytoluene-PUF	Cd(II)	0.32	100	[67]
Acetylacetone phenylhydrazone-PUF	Cu(II)	0.80	100	[68]
Alizarin Red S-Amberlite XAD-2	Cd(II)	0.12	40	[65]
Diacetyl monoxime-Silica gel	Cu(II)	0.42	100	[69]
Organobentonite/iron oxide/PUF nanocomposite	Cd(II)	7.80	–	[43]
Starch-graft-acrylic acid/Montmorillonite nanocomposite	Cu(II)	3.18	–	[70]
Nanosize titanate	Cu(II)	13.8	–	[71]
	Cd(II)	8.8		
Sawdust chitosan nanocomposite	Cu(II)	7.30	–	[72]
Polyaniline/calcium alginate	Cu(II)	0.25		[73]
Maghemite-magnetite nanocomposite	Cd(II)	2.70	–	[74]
Magnetic oak wood char composite	Cd(II)	2.90	–	[75]
Carbon nanotubes, nanofibers, activated carbon and fly ash	Cd(II)	1.22–2.02	–	[76]

nanocomposite will increase the capacity, which will be the subject of our next study. Despite this, other characteristics such as low cost, ease of preparation, and low detection limit make this material suitable for adsorption and removal of these elements in low concentration water samples. Advantageously, the obtained CF value is higher than that of all the mentioned preconcentration sorbents, making the proposed material a viable option for removing Cu and Cd from water samples even in complex matrices. This also confirms the efficacy of using this material in analytical applications and increases the concentration of elements in the sample to the required level for measurement.

5. Conclusions

The chemical embedding of $Zn_{0.6}Mn_{0.4}Fe_2O_4$ nanoparticles in PUF resulted in the development of a new polymeric nanocomposite sorbent for the adsorptive removal of Cu and Cd from aqueous solutions. The resulting ferrite nanoparticles and nanocomposite materials were investigated. Based on the XRD data, the synthesized $Zn_{0.6}Mn_{0.4}Fe_2O_4$ nanoparticles demonstrated high crystallinity and purity of the spinel phase, with an average crystallite size of all nanoparticles of about 16.6 nm. Also, a high saturation magnetization (M_s) value of 6.9 emu g^{-1} was obtained. The HR-TEM images of the polymeric nanocomposite revealed that the nanoparticles are scattered in the PUF and/or agglomerated together within the PUF due to the magnetic nature of the ferrite nanoparticles. However, the embedding during the foaming process of PUF support has reduced the dense agglomeration of the nanoparticles. The embedded nanoparticles in the $Zn_{0.6}Mn_{0.4}Fe_2O_4$/PUF nanocomposite varied in size from ~5.3 to 18.5 nm. The microstructure of the prepared $Zn_{0.6}Mn_{0.4}Fe_2O_4$/PUF composite had a spherically shaped spongy structure of higher porosity. The best adsorption for Cu and Cd was obtained at a solution pH of 6.5, a shaking time of 60 min, and an adsorbent dosage of 0.2 g. The adsorption kinetics adopted the diffusion-controlled and pseudo-second-order kinetic models due to the presence of micropores and macropores in the structures of the polymeric nanocomposite material. A composite dosage of 0.2 g was found suitable for maximum adsorption efficiency and higher uptake. The maximum adsorption capacity was found to be 1.84 and 1.19 mg g^{-1} for Cu and Cd, respectively. The adsorption isotherm was best fitted with the Freundlich model. The preconcentration factor was 125 for the two elements. The limit of quantification obtained was 0.9 and 1.4 µg L^{-1}. Desorption and reusability revealed that sorption performance remained unchanged after 5.0 regeneration cycles. The adsorption findings clearly showed the usefulness of the $Zn_{0.6}Mn_{0.4}Fe_2O_4$/PUF nanocomposite for effective Cu and Cd adsorption/removal from water. The synthesis method is very simple, low-cost, and environmentally-safe, and the sorbent obtained has high selectivity and tolerance to foreign ions. The use of the low-cost PUF as support and reluctance for the nanoparticle agglomeration is a positive, making it an economically effective adsorbent. The adsorption capacity and CF were found to be sufficient for use with real water samples, rendering it an alternate trace element adsorbent.

Declaration of interest

The authors declare no potential conflict of interest.

Data availability statement

The data supporting the findings of this work are available from the corresponding author (Sami Abdel Azeem), upon reasonable request.

References

[1] K.R. Awad, M.M.S. Wahsh, S.T. El-Wakeel, K.I. Ochiabuto, A.G.M. Othman, I.Y. El-Sherif, $Mn_{0.2}Co_{0.8}Fe_2O_4$ and encapsulated $Mn_{0.2}Co_{0.8}Fe_2O_4/SiO_2$ magnetic nanoparticles for efficient Pb^{2+} removal from aqueous solution, Water Sci. Technol., 80 (2019) 377–386.

[2] L.M. Gaetke, C.K. Chow, Copper toxicity, oxidative stress, and antioxidant nutrients, Toxicology, 189 (2003) 147–163.

[3] C.E. Chubaka, H. Whiley, J.W. Edwards, K.E. Ross, Lead, zinc, copper, and cadmium content of water from South Australian rainwater tanks, Int. J. Environ. Res. Public Health, 15 (2018) 1551, doi: 10.3390/ijerph15071551.

[4] S. Chatterjee, S. Sarkar, S. Bhattacharya, Toxic metals and autophagy, Chem. Res. Toxicol., 27 (2014) 1887–1900.

[5] WHO, Guidelines for Drinking-Water Quality, 3rd ed., Incorporating the First and Second Addenda, Vol. 1, Recommendations, World Health Organization, Geneva, 2008.

[6] D.A. Glatstein, F.M. Francisca, Influence of pH and ionic strength on Cd, Cu and Pb removal from water by adsorption in Na-bentonite, Appl. Clay Sci., 118 (2015) 61–67.

[7] Y. Ma, Z. Deng, Z. Li, Q. Lin, Y. Wu, W. Dou, Adsorption characteristics and mechanism for $K_2Ti_4O_9$ whiskers removal of Pb(II), Cd(II), and Cu(II) cations in wastewater, J. Environ. Chem. Eng., 9 (2021) 106236, doi: 10.1016/j.jece.2021.106236.

[8] H. Li, H. Ji, X. Cui, X. Che, Q. Zhang, J. Zhong, R. Jin, L. Wang, Y. Luo, Kinetics, thermodynamics, and equilibrium of As(III), Cd(II), Cu(II) and Pb(II) adsorption using porous chitosan bead-supported $MnFe_2O_4$ nanoparticles, Int. J. Min. Sci. Technol., 31 (2021) 1107–1115.

[9] F. Valenzuela, G. Quintana, A. Briso, V. Ide, C. Basualto, J. Gaete, G. Montes, Cu(II), Cd(II), Pb(II) and As(V) adsorption from aqueous solutions using magnetic iron-modified calcium silicate hydrate: adsorption kinetic analysis, J. Water Process Eng., 40 (2021) 101951, doi: 10.1016/j.jwpe.2021.101951.

[10] I.V. Joseph, L. Tosheva, A.M. Doyle, Simultaneous removal of Cd(II), Co(II), Cu(II), Pb(II), and Zn(II) ions from aqueous solutions via adsorption on FAU-type zeolites prepared from coal fly ash, J. Environ. Chem. Eng., 8 (2020) 103895, doi: 10.1016/j.jece.2020.103895.

[11] Y. Zhang, L. Zhang, R. Gao, L. Zhong, J. Xue, $CaCO_3$-coated PVA/BC-based composite for the simultaneous adsorption of Cu(II), Cd(II), Pb(II) in aqueous solution, Carbohydr. Polym., 267 (2021) 118227, doi: 10.1016/j.carbpol.2021.118227.

[12] Y. Zhang, Y. Wang, H. Zhang, Y. Li, Z. Zhang, W. Zhang, Recycling spent lithium-ion battery as adsorbents to remove aqueous heavy metals: adsorption kinetics, isotherms, and regeneration assessment, Resour. Conserv. Recycl., 156 (2020) 104688, doi: 10.1016/j.resconrec.2020.104688.

[13] J.M. Silva, B.S. Farias, D.D.R. Gründmann, T.R.S. Cadaval Jr., J.M. Moura, G.L. Dotto, L.A.A. Pinto, Development of chitosan/*Spirulina* bio-blend films and its biosorption potential for dyes, J. Appl. Polym. Sci., 134 (2017) 44580, 1–8, doi: 10.1002/app.44580.

[14] R. Laus, T.G. Costa, B. Szpoganicz, V.T. Fávere, Adsorption and desorption of Cu(II), Cd(II) and Pb(II) ions using chitosan crosslinked with epichlorohydrin-triphosphate as the adsorbent, J. Hazard. Mater., 183 (2010) 233–241.

[15] S. Lata, S.R. Samadder, Removal of arsenic from water using nano adsorbents and challenges: a review, J. Environ. Manage., 166 (2016) 387–406.

[16] Q.-Z. Zhai, Use of SBA-15 ordered nano mesoporous silica for removal of copper(II) from aqueous media: studies on equilibrium, isotherm, kinetics and thermodynamics, J. Environ. Chem. Eng., 7 (2019) 103069, 1–9, doi: 10.1016/j.jece.2019.103069.

[17] A.I.A. Sherlala, A.A.A. Raman, M.M. Bello, A. Asghar, A review of the applications of organo-functionalized magnetic graphene oxide nanocomposites for heavy metal adsorption, Chemosphere, 193 (2018) 1004–1017.

[18] Y. Harinath, D. Harikishore Kumar Reddy, L. Subramanyam Sharma, K. Seshaiah, Development of hyperbranched polymer encapsulated magnetic adsorbent ($Fe_3O_4@SiO_2$–NH_2-PAA) and its application for decontamination of heavy metal ions, J. Environ. Chem. Eng., 5 (2017) 4994–5001.

[19] D. Cai, T.L. Zhang, F.J. Zhang, X.M. Luo, Quaternary ammonium beta-cyclodextrin-conjugated magnetic nanoparticles as nano-adsorbents for the treatment of dyeing wastewater: synthesis and adsorption studies, J. Environ. Chem. Eng., 5 (2017) 2869–2878.

[20] A.S. Adeleye, J.R. Conway, K. Garner, Y.X. Huang, Y.M. Su, A.A. Keller, Engineered nanomaterials for water treatment and remediation: costs, benefits, and applicability, J. Chem. Eng., 286 (2016) 640–662.

[21] Z. Jiang, Y. Zhao, P. Yang, Formation of MFe_2O_4 (M = Co, Mn, Ni) 1D nanostructures towards rapid removal of pollutants, Mater. Chem. Phys., 214 (2018) 1–7.

[22] W. Sun, W. Pan, F. Wang, N. Xu, Removal of Se(IV) and Se(VI) by MFe_2O_4-nanoparticles from aqueous solution, Chem. Eng. J., 273 (2015) 353–362.

[23] N.U. Yamaguchi, R. Bergamasco, S. Hamoudi, Magnetic $MnFe_2O_4$-graphene hybrid composite for efficient removal of glyphosate from water, Chem. Eng. J., 295 (2016) 391–402.

[24] K.K. Das, S. Patnaik, B. Nanda, A.C. Pradhan, K. Parida, $ZnFe_2O_4$-decorated mesoporous Al_2O_3 modified MCM-41: a solar-light-active photocatalyst for the effective removal of phenol and Cr(VI) from water, ChemistrySelect, 4 (2019) 1806–1819.

[25] M. Alaqarbeh, F.I. Khalili, O. Kanoun, Manganese ferrite ($MnFe_2O_4$) as potential nanosorbent for adsorption of uranium(VI) and thorium(IV), J. Radioanal. Nucl. Chem., 323 (2020) 515–537.

[26] Z. Ai, Y. Cheng, L. Zhang, J. Qiu, Efficient removal of Cr(VI) from aqueous solution with $Fe@Fe_2O_3$ core-shell nanowires, Environ. Sci. Technol., 42 (2008) 6955–6960.

[27] K.K. Das, S.P. Tripathy, K. Parida, Adsorption study of hexavalent chromium by porous and non-porous $ZnFe_2O_4$, Mater. Today:. Proc., 35 (2020) 289–293.

[28] B. Eyvazi, A. Jamshidi-Zanjani, A.K. Darban, Immobilization of hexavalent chromium in contaminated soil using nano-magnetic $MnFe_2O_4$, J. Hazard. Mater., 365 (2019) 813–819.

[29] Y. Ren, N. Li, J. Feng, T. Luan, Q. Wen, Z. Li, M. Zhang, Adsorption of Pb(II) and Cu(II) from aqueous solution on magnetic porous ferrospinel $MnFe_2O_4$, J. Colloid Interface Sci., 367 (2012) 415–421.

[30] Z. Beji, A. Hanini, L.S. Smiri, J. Gavard, K. Kacem, F. Villain, J.-M. Grenèche, F. Chau, S. Ammar, Magnetic properties of Zn-substituted $MnFe_2O_4$ nanoparticles synthesized in polyol as potential heating agents for hyperthermia. Evaluation of their toxicity on Endothelial cells, Chem. Mater., 22 (2010) 5420–5429.

[31] A.M. Jacintha, V. Umapathy, P. Neeraja, S.R.J. Rajkumar, Synthesis and comparative studies of $MnFe_2O_4$ nanoparticles with different natural polymers by solegel method: structural, morphological, optical, magnetic, catalytic and biological activities, J. Nanostruct. Chem., 7 (2017) 375–387.

[32] J. Wang, C. Zeng, Z. Peng, Q. Chen, Synthesis and magnetic properties of $Zn_{1-x}Mn_xFe_2O_4$ nanoparticles, Physica B, 349 (2004) 124–128.

[33] B.R. Vergis, R. Hari Krishna, N. Kottam, B.M. Nagabhushana, R. Sharath, B. Darukaprasad, Removal of malachite green from aqueous solution by magnetic $CuFe_2O_4$ nano-adsorbent synthesized by one pot solution combustion method, J. Nanostruct. Chem., 8 (2018) 1–12.

[34] P. Thakur, D. Chahar, S. Taneja, N. Bhalla, A. Thakur, A review on MnZn ferrites: synthesis, characterization and applications, Ceram. Int., 46 (2020) 15740–15763.

[35] M.-R. Huang, S.-J. Huang, X.-G. Li, Facile synthesis of polysulfoaminoanthraquinone nanosorbents for rapid removal and ultrasensitive fluorescent detection of heavy metal ions, J. Phys. Chem. C, 115 (2011) 5301–5315.

[36] N. Burham, Separation and preconcentration system for lead and cadmium determination in natural samples using 2-aminoacetylthiophenol modified polyurethane foam, Desalination, 249 (2009) 1199–1205.

[37] A.N. Anthemidis, G.A. Zachariadis, J.A. Stratis, On-line preconcentration and determination of copper, lead and chromium(VI) using unloaded polyurethane foam packed column by flame atomic absorption spectrometry in natural waters and biological samples, Talanta, 58 (2002) 831–840.

[38] M.F. El-Shahat, E.A. Moawed, M.A.A. Zaid, Preconcentration and separation of iron, zinc, cadmium and mercury, from waste water using Nile blue a grafted polyurethane foam, Talanta, 59 (2003) 851–866.

[39] S.M. Abdel Azeem, H.A. Hanafi, Y. El-Nadi, M.F. El-Shahat, Separation of nickel and cadmium from aqueous solutions by flow injection preconcentration onto cadion functionalized polyurethane foam, Microchem. J., 166 (2021) 106192, doi: 10.1016/j.microc.2021.106192.

[40] S.M. Abdel Azeem, W.A.A. Arafa, M.F. El-Shahat, Synthesis and application of alizarin complexone functionalized polyurethane foam: preconcentration/separation of metal ions from tap water and human urine, J. Hazard. Mater., 182 (2010) 286–294.

[41] N. Danesh, M. Ghorbani, A. Marjani, Separation of copper ions by nanocomposites using adsorption process, Sci. Rep., 11 (2021) 1676, doi: 10.1038/s41598-020-80914-w.

[42] M. Sayed, N. Burham, Removal of cadmium(II) from aqueous solution and natural water samples using polyurethane foam/organobentonite/iron oxide nanocomposite adsorbent, Int. J. Environ. Sci. Technol., 15 (2018) 105–118.

[43] J. Azadmanjiri, Preparation of Mn–Zn ferrite nanoparticles from chemical sol–gel combustion method and the magnetic properties after sintering, J. Non-Cryst. Solids, 353 (2007) 4170–4173.

[44] A. Teber, K. Cil, T. Yilmaz, B. Eraslan, D. Uysal, G. Surucu, A.H. Baykal, R. Bansal, Manganese and zinc spinel ferrites blended with multi-walled carbon nanotubes as microwave absorbing materials, Aerospace, 4 (2017) 2, doi: 10.3390/aerospace4010002.

[45] S. Pandey, S. Tiwari, Facile approach to synthesize chitosan based composite—characterization and cadmium(II) ion adsorption studies, Carbohydr. Polym., 134 (2015) 646–656.

[46] A. Gundogdu, C. Duran, H.B. Senturk, M. Soylak, M. Imamoglud, Y. Onal, Physico-chemical characteristics of a novel activated carbon produced from tea industry waste, J. Anal. Appl. Pyrolysis, 104 (2013) 249–259.

[47] G. Sharma, Mu. Naushad, Adsorptive removal of noxious cadmium ions from aqueous medium using activated carbon/zirconium oxide composite: isotherm and kinetic modeling, J. Mol. Liq., 310 (2020) 113025, doi: 10.1016/j.molliq.2020.113025.

[48] K. Szewczuk-Karpisz, M. Wiśniewska, M. Medykowska, M.V. Galaburda, V.M. Bogatyrov, O.I. Oranska, M. Błachnio, P. Oleszczuk, Simultaneous adsorption of Cu(II) ions and poly(acrylic acid) on the hybrid carbon-mineral nanocomposites with metallic elements, J. Hazard. Mater., 412 (2021) 125138, doi: 10.1016/j.jhazmat.2021.125138.

[49] S. Palagyi, T. Braun, Unloaded polyether type polyurethane foams as solid extractants for trace elements, J. Radioanal. Nucl. Chem., 163 (1992) 69–79.

[50] L.V.A. Gurgel, J.C.P. de Melo, J.C. de Lena, L.F. Gil, Adsorption of chromium(VI) ion from aqueous solution by succinylated mercerized cellulose functionalized with quaternary ammonium groups, Bioresour. Technol., 100 (2009) 3214–3220.

[51] Y.S. Ho, G. McKay, D.A.J. Wase, C.F. Forster, Study of the sorption of divalent metal ions on to peat, Adsorpt. Sci. Technol., 18 (2000) 639–650.

[52] W.J. Weber Jr., J. Carrell Morris, Kinetics of adsorption on carbon from solution, J. Sanit. Eng. Div., 89 (1963) 31–59.

[53] I. Langmuir, The adsorption of gases on plane surfaces of glass, mica and platinum, J. Am. Chem. Soc., 40 (1918) 1361–1403.

[54] H.M.F. Freundlich, Over the adsorption in solution, J. Phys. Chem., 57 (1906) 385–470.

[55] M. Kondalkar, U. Fegade, Inamuddin, S. Kanchi, T. Altalhi, K.E. Suryawanshi, A.M. Patil, Adsorption of Cr(VI) on ultrafine Al_2O_3-doped $MnFe_2O_4$ nanocomposite surface: experimental and theoretical study using double-layer modeling, J. Phys. Chem. Solids, 163 (2022) 110544, doi: 10.1016/j.jpcs.2021.110544.

[56] Z. Tu, Q. He, X. Chang, Z. Hu, R. Gao, L. Zhang, Z. Li, 1-(2-Formamidoethyl)-3-phenylurea functionalized activated carbon for selective solid-phase extraction and preconcentration of metal ions, Anal. Chim. Acta, 649 (2009) 252–257.

[57] A. Ivanets, V. Prozorovich, T. Kouznetsova, T. Dontsova, O. Yanushevska, A. Hosseini-Bandegharaei, V. Srivastava, M. Sillanpää, Effect of Mg^{2+} ions on competitive metal ions adsorption/desorption on magnesium ferrite: mechanism, reusability and stability studies, J. Hazard. Mater., 411 (2021) 124902, doi: 10.1016/j.jhazmat.2020.124902.

[58] C. Teodosiu, R. Wenkert, L. Tofan, C. Paduraru, Advances in preconcentration/removal of environmentally relevant heavy metal ions from water and wastewater by sorbents based on polyurethane foam, Rev. Chem. Eng., 30 (2014) 403–420.

[59] K. Prasad, P. Gopikrishna, R. Kala, T. Prasada Rao, G.R.K. Naidu, Solid phase extraction vis-à-vis coprecipitation preconcentration of cadmium and lead from soils onto 5,7-dibromoquinoline-8-ol embedded benzophenone and determination by FAAS, Talanta, 69 (2006) 938–945.

[60] N. Burham, M. Sayed, Adsorption behavior of Cd^{2+} and Zn^{2+} onto natural Egyptian bentonitic clay, Minerals, 6 (2016) 129, 1–15, doi: 10.3390/min6040129.

[61] H. Radnia, A.A. Ghoreyshi, H. Younesi, G.D. Najafpour, Adsorption of Fe(II) ions from aqueous phase by chitosan adsorbent: equilibrium, kinetic, and thermodynamic studies, Desal. Water Treat., 50 (2012) 348–359.

[62] K. Hasegawa, K. Minakata, M. Suzuki, O. Suzuki, The standard addition method and its validation in forensic toxicology, Forensic Toxicol., 39 (2021) 311–333.

[63] N. Burham, S.R. Abdel-Hafeez, S.M. Abdel-Azeem, M.F. El-Shahat, Retention profile of Fe, Mn and Cu onto chemically treated polyurethane with carbon disulfide, Int. J. Environ. Anal. Chem., 93 (2013) 1413–1427.

[64] R. Saxena, A.K. Singh, S.S. Sambi, Synthesis of a chelating polymer matrix by immobilizing Alizarin Red-S on Amberlite XAD-2 and its application to the preconcentration of lead(II), cadmium(II), zinc(II) and nickel(II), Anal. Chim. Acta, 295 (1994) 199–204.

[65] N.B. Burham, S.M. Abdel Azeem, S.R. Abdel-Hafeze, M.F. El-Shahat, Determination of trace metal ions in water and plant samples using polyurethane foam modified with 2-aminothiazole, Desal. Water Treat., 56 (2015) 3024–3035.

[66] N. Burham, S.M. Abdel-Azeem, M.F. El-Shahat, Separation and determination of trace amounts of zinc, lead, cadmium and mercury in tap and Qaroun Lake water using polyurethane foam functionalized with 4-hydroxytoluene and 4-hydroxyacetophenone, Anal. Chim. Acta, 579 (2006) 193–201.

[67] S.M. Abdel Azeem, S.M. Mohamed Attaf, M.F. El-Shahat, Acetylacetone phenylhydrazone functionalized polyurethane foam: determination of copper, zinc and manganese in environmental samples and pharmaceutics using flame atomic absorption spectrometry, React. Funct. Polym., 73 (2013) 182–191.

[68] S.M. Abdel Azeem, S.M. Attaf, M.F. El–Shahat, Solid-phase extraction of Cu, Zn, and Mn from Nile river and tap water prior to flame atomic absorption determination, Desal. Water Treat., 57 (2016) 21893–21903.

[69] G. Güçlü, E. Al, S. Emik, T.B. İyim, S. Özgümüş, M. Özyürek, Removal of Cu^{2+} and Pb^{2+} ions from aqueous solutions by starch-graft-acrylic acid/montmorillonite superabsorbent nanocomposite hydrogels, Polym. Bull., 65 (2010) 333–346.

[70] A. Wang, Y. Si, H. Yin, J. Chen, J. Huo, Synthesis of Na-, Fe-, and Mg-containing titanate nanocomposites starting from ilmenite and NaOH and adsorption kinetics, isotherms, and

thermodynamics of Cu(II), Cd(II), and Pb(II) cations, Mater. Sci. Eng. B, 249 (2019) 114411, doi: 10.1016/j.mseb.2019.114411.

[71] K. Kayalvizhi, N.M.I. Alhaji, D. Saravanakkumar, S. Beer Mohamed, K. Kaviyarasu, A. Ayeshamariam, A.M. Al-Mohaimeed, M.R. AbdelGawwad, M.S. Elshikh, Adsorption of copper and nickel by using sawdust chitosan nanocomposite beads – a kinetic and thermodynamic study, Environ. Res., 203 (2022) 111814, doi: 10.1016/j.envres.2021.111814.

[72] N. Jiang, Y. Xu, Y. Dai, W. Luo, L. Dai, Polyaniline nanofibers assembled on alginate microsphere for Cu^{2+} and Pb^{2+} uptake, J. Hazard. Mater., 215–216 (2012) 17–24.

[73] N. Kataria, V.K. Garg, Green synthesis of Fe_3O_4 nanoparticles loaded sawdust carbon for cadmium(II) removal from water: regeneration and mechanism, Chemosphere, 208 (2018) 818–828.

[74] D. Mohan, H. Kumar, A. Sarswat, M. Alexandre-Franco, C.U. Pittman Jr., Cadmium and lead remediation using magnetic oak wood and oak bark fast pyrolysis bio-chars, Chem. Eng. J., 236 (2014) 513–528.

[75] Ihsanullah, F.A. Al-Khaldi, B. Abusharkh, M. Khaled, M.A. Atieh, M.S. Nasser, T. laoui, T.A. Saleh, S. Agarwal, I. Tyagie V.K. Gupta, Adsorptive removal of cadmium(II) ions from liquid phase using acid modified carbon-based adsorbents, J. Mol. Liq., 204 (2015) 255–263.

[76] A. Shahat, M.R. Awual, Mu. Naushad, Functional ligand anchored nanomaterial based facial adsorbent for cobalt(II) detection and removal from water samples, Chem. Eng. J., 271 (2015) 155–163.